Article:
Charlton, FW, Hover, S orcid.org/0000-0001-9190-5670, Fuller, J orcid.org/0000-0001-8801-149X et al. (4 more authors) (2019) Cellular cholesterol abundance regulates potassium accumulation within endosomes and is an important determinant in bunyavirus entry. Journal of Biological Chemistry, 294 (18). pp. 7335-7347. ISSN 0021-9258

https://doi.org/10.1074/jbc.ra119.007618

Cellular cholesterol abundance regulates potassium accumulation within endosomes and is an important determinant in Bunyavirus entry

Frank W. Charlton, Samantha Hover, Jack Fuller, Roger Hewson, Juan Fontana, John N. Barr, Jamel Mankouri

[1]School of Molecular and Cellular Biology, University of Leeds, Leeds, United Kingdom, LS2 9JT
[2]Astbury Centre for Structural Molecular Biology, University of Leeds, United Kingdom, LS2 9JT
[3]National Infection Service, Public Health England, Porton Down, Salisbury, United Kingdom, SP4 0JG

Running title: Cellular cholesterol regulates endosomal K^+ and bunyavirus entry

Key words: virus entry; cholesterol; potassium ions; ion channels; sterol metabolism; bunyavirus; membrane fusion; endosome; endocytic membrane network; membrane gradient.

Corresponding authors: John N Barr and Jamel Mankouri

To whom correspondence should be addressed: John N. Barr : School of Molecular and Cellular Biology, University of Leeds, Leeds, United Kingdom, LS2 9JT; (j.n.barr@leeds.ac.uk); Tel: +44 113 3438069. Jamel Mankouri: School of Molecular and Cellular Biology, University of Leeds, Leeds, United Kingdom, LS2 9JT; (j.mankouri@leeds.ac.uk); Tel: +44 113 3435646.

ABSTRACT

The Bunyavirales order of segmented negative-sense RNA viruses includes > 500 isolates that infect insects, animals, and plants and are often associated with severe and fatal disease in humans. To multiply and cause disease, bunyaviruses must translocate their genomes from outside the cell into the cytosol, achieved by transit through the endocytic network. We have previously shown that the model bunyaviruses Bunyamwera virus (BUNV) and Hazara virus (HAZV) exploit the changing potassium concentration ($[K^+]$) of maturing endosomes to release their genomes at the appropriate endosomal location. K^+ was identified as a biochemical cue to activate the viral fusion machinery, promoting fusion between viral and cellular membranes, consequently permitting genome release. In this study, we further define the biochemical prerequisites for BUNV and HAZV entry and their K^+ dependence. Using drug–mediated cholesterol extraction along with viral-entry and K^+ uptake assays, we report three major findings: (1) BUNV and HAZV require cellular cholesterol during endosomal escape; (2) cholesterol depletion from host cells impairs K^+ accumulation in maturing endosomes, revealing new insights into endosomal K^+ homeostasis; and (3) "priming" BUNV and HAZV virions with K^+ before infection alleviates

their cholesterol requirement. Taken together, our findings suggest a model in which cholesterol abundance influences endosomal K^+ levels and consequently the efficiency of bunyavirus infection. The ability to inhibit bunyaviruses with existing cholesterol-lowering drugs may offer new options for future antiviral interventions for pathogenic bunyaviruses.

Word count: 231

INTRODUCTION

The order Bunyavirales represents the largest taxonomic collection of single-stranded, negative-sense RNA (-ssRNA) viruses, with over 500 named isolates, classified into 10 families and 35 genera (1). Bunyaviruses infect a wide range of hosts including animals, plants, insects and humans. Those viruses able to infect humans are classified into just four of the bunyavirales families, namely Hantaviridae, Phenuiviridae, Nairoviridae and Peribunyaviridae, with selected species able to cause potentially fatal haemorrhagic fever or encephalitis in their human hosts (2).

The genome of all bunyaviruses comprises three linear RNA segments that are named according to their relative size, with the large (L) segment encoding the viral RdRp, the medium (M) segment encoding envelope-associated glycoproteins (Gn and Gc) and the small (S) segment encoding the nucleoprotein (N), which encapsidates the RNA segments to form ribonucleoprotein complexes (RNPs). In many bunyavirus species, an additional non-structural protein (NSs) is expressed from the S segment either from an overlapping open reading frame on the N mRNA, or alternatively via the generation of a discrete mRNA through ambi-sense transcription (3). Many bunyaviruses also express a non-structural protein from the M segment (NSm) which is cleaved from the single polyprotein precursor transcribed from the single M segment mRNA (4–6).

For bunyaviruses to establish infection, they must penetrate host cells and traverse the endocytic network, prior to escape of viral RNPs into the cytosol and subsequent gene expression. Cell penetration of bunyaviruses occurs through attachment of the virus to the cell, followed by internalisation through a range of mechanisms. It is known that viruses of the families Hantaviridae, Nairoviridae and Peribunyaviridae are endocytosed through a clathrin-dependent mechanism, with functional roles for caveolar endocytosis and macropinocytosis also described. Conversely, viruses of the Phenuiviridae enter cells independently of clathrin (7–10). Once inside endosomes, bunyaviruses must facilitate the escape of their RNPs into the cytosol, a process involving the fusion of the virus envelope with the endosomal membrane. This fusion event is mediated by the heteromultimeric glycoprotein spikes comprising Gn and Gc, arranged on the surface of mature virions in a variety of different architectures (11–14). For the fusion machinery to be activated, the glycoprotein spikes must be subjected to a variety of specific biochemical events that can occur before or after their inclusion in the virion. For instance, most class I and II fusion proteins studied to date require a proteolytic cleavage event to become fusion competent (15). This event is termed ‘priming’, after which a variety of further events known as ‘triggers’ induce structural changes in the fusion proteins resulting in a transition between pre- and post-fusion conformations. While the priming step involves proteolysis, there is a greater variety of triggers including pH and the interaction with an internal or external cellular receptor. These triggering events ensure that fusion between viral and cellular membranes is restricted only to an appropriate cellular location that leads to productive infection (15).

Recently, we used the prototypic bunyavirus, Bunyamwera virus (BUNV), and the model nairovirus Hazara virus (HAZV) to reveal that bunyavirus fusion is dependent upon specific changes in both pH and ion balance (16, 17). Specifically, we identified K^+ as a critical biochemical trigger required for spike conformational changes and interaction with membranes, consistent with activation of the fusogenic machinery. While this work documented how bunyavirus glycoproteins respond to specific endosomal conditions, it is likely that efficient fusion between virus and endosomal membranes requires further biochemical requirements as pre-requisites for virus entry. In this regard, it is known that the composition of biological membranes is crucial to the physiological function of cells, and cholesterol is an important regulator of membrane integrity and fluidity, making up 25-50% of the total lipid content of animal cells (18). Aberrations in cholesterol homeostasis can disrupt cellular uptake mechanisms, which is important from the view of enveloped viruses. The correct composition of biological membranes in terms of cholesterol has been shown to be important to the life cycle of several enveloped viruses, in a variety of lifecycle stages ranging from entry to release. As well as the correct environmental pH, the Togaviridae family member Semliki Forest virus (SFV), requires high cholesterol composition in target membranes for stable insertion of its fusion loop (19), whilst the hantavirus Andes virus (ANDV) has been demonstrated to require high cholesterol in target membranes for productive infection (20). Cholesterol concentrations also influence the hemifusion stage of influenza virus (IAV) fusion (21). Aside from the entry stages of viral life cycles, cholesterol has been shown to be important in the assembly and release of mature IAV virions which require cholesterol to stabilise virions prior to release (22).

In this study, we examined how the biochemical composition of both host and viral membranes influences the crucial fusion step in the bunyavirus life cycle. Herein, we reveal new insights into the role of cholesterol during virion endocytic trafficking and endosomal K^+ accumulation.

RESULTS

BUNV infection is inhibited by cellular cholesterol depletion

Given that enveloped viruses must fuse their outer membranes with host membranes to cause infection (23), we first examined if cholesterol, a key regulator of membrane fluidity (24), has a role in this process. Cholesterol-rich microdomains within the plasma membrane are important for the lifecycle of a range of enveloped viruses, but their role during the bunyavirus lifecycle is poorly characterised.

In the following experiments, cellular cholesterol was extracted from the plasma membrane of BUNV-susceptible A549 cells using methyl-beta cyclodextrin (MβCD) and its influence on BUNV infection assessed (Fig 1). Cells were treated with MβCD for 45 minutes to sequester cellular cholesterol, and incubated with BUNV (MOI = 0.2) for 2 h to permit virus penetration. Non-internalised viruses were removed 2 hrs post-infection (hpi) through trypsin washing, and the ability of BUNV to establish an infection after 24 hrs was assessed through the detection of BUNV-N by immunofluorescence staining (Fig 1A and B). Quantification of cells positive for BUNV-N revealed significantly reduced levels of infection upon MβCD treatment (reduction to ~29%) (Fig 1B, black bars). When BUNV infection was assessed at varying concentrations of MβCD (0.5-2 mM) by western blotting (Fig 1C and D), N expression was barely detectable at 0.5-1 mM, and completely undetectable at 2 mM MβCD (Fig 1C), revealing a concentration dependent decrease (Fig 1D, black bars). Importantly, MβCD treatment was non-cytotoxic, evidenced through MTS assays (Fig 1B and 1D, grey bars) and the equivalent levels of GAPDH in the corresponding protein lysates (Fig 1C).

To confirm the BUNV cholesterol requirement, the effects of PF-429242 (S1P/SKI-1 inhibitor) (25), and U-18666A (lysosomal cholesterol export inhibitor) (26) that reduce cellular cholesterol through the inhibition of its production and trafficking respectively, were assessed (Fig 1E-H). Both PF-429242 and siRNA-mediated S1P inhibition have been shown to inhibit Andes virus (ANDV) (27), whilst U-18666A has inhibitory effects on a number of important enveloped viruses, including dengue virus (DENV), chikungunya virus (CHIKV) and Ebola virus (EBOV) (28–30). For these experiments, cells were pre-treated with PF-429242 for 24 hours (31) and infected with BUNV (MOI 0.2, 24 h). Ammonium chloride (NH_4Cl), a known inhibitor of BUNV fusion was included in these assays as a positive control (16). PF-429242 at 20 μM resulted in almost complete abrogation of BUNV-N production, whilst 5-10 μM led to drastically reduced BUNV-N expression (Fig 1E). Quantification revealed that the BUNV-N levels decreased to 7.91%, 17.54% and 37.94% in 20, 10 and 5 μM drug-treated cells respectively, compared to the no-drug control (Fig 1F; black bars). MTS assays revealed no detrimental effects of PF-429242 on cell viability (Fig 1F, grey bars).

For further confirmation, cells were treated with U-18666A under identical conditions (26). Fig 1G shows a strong inhibition of BUNV in cells treated with 5-10 μM U-18666A and more modest inhibition at 2.5 μM U-18666A. Upon quantification (Fig 1H, black bars), BUNV-N expression was reduced to 8.52%, 22.83% and 42.66% by 10, 5 and 2.5 μM U18666A, respectively. MTS assays confirmed no loss of viability at the U18666A concentrations assessed (Fig 1H, grey bars).

Finally, we assessed cholesterol depletion as a viable anti-BUNV strategy through assessment of the inhibitory effects of the clinically approved cholesterol lowering drug simvastatin. Fig 1I-J shows that BUNV-N expression was reduced by 50, 35, 20 and 10 μM simvastatin treatment to 24.74%, 34.29%, 38.82% and 48.37% respectively, when normalised to no-drug

controls. MTS assays confirmed no drug induced cytotoxicity (Fig 1J, grey bars). Taken together, these data obtained via four independent methods strongly suggest that cholesterol is important during the BUNV lifecycle and that clinically-approved cholesterol-lowering drugs hold promise as a clinically available antiviral strategy.

Both virion envelope and cellular cholesterol influence BUNV infection

As BUNV is an enveloped virus, we next assessed whether envelope cholesterol contributed to the effects of cholesterol lowering compounds. To assess this, we used a recombinant BUNV containing GFP inserted at the N-terminus of a truncated Gc glycoprotein (GFP-Gc) with the deleted sequence shown to be dispensable for virus infection in cell culture (32, 33). GFP-BUNV virions were treated in vitro with MβCD for 90 minutes at 37°C to sequester cholesterol from the virion membrane (Fig 2A). To mitigate the effects of MβCD on the cells, virions were diluted in media prior to infection (MOI 0.5, 24 hrs). This ensured that any effects of cholesterol depletion were mediated by direct effects on the virions as opposed to cellular effects.

From these experiments, we observed a ~24% decrease in total BUNV-N expression following direct MβCD virion treatment (Fig 2B-C) by western blot analysis. Upon the assessment of GFP-Gc fluorescence (34) (Fig 2D), a larger ~60% decrease in the number of infected cells was observed (Fig 2E). This confirmed that MβCD virion treatment decreased the number of infected cells. The ultrastructure of BUNV virions was unaffected by cholesterol depletion as negative staining showed no gross structural defects in the virions following MβCD treatment (Fig 2F). We therefore reasoned that BUNV infection is dependent on virion as well as cellular associated cholesterol.

Cellular cholesterol depletion influences BUNV endocytic escape but not cell penetration

To further dissect the role of cholesterol during BUNV infection and identify the steps at which MβCD-mediated cholesterol extraction inhibits the virus lifecycle, time of addition assays were performed. We included NH_4Cl, an endosomal acidification inhibitor, as a control which inhibits BUNV at early stages of infection, i.e. only during its movement through the endocytic system (16). Cells were infected with BUNV (MOI 0.2) (t=0) and NH_4Cl or MβCD were added to cells at defined time points up to and including 10 hpi. Infection was then allowed to proceed until 24 hpi and BUNV-N expression assessed (Fig 3A-B). Figs 3A and C show that BUNV escapes from endosomes at or before 6 hpi, as NH_4Cl treatment did not influence BUNV-N production when added ≥6 hpi, consistent with our previous findings (16). Interestingly, BUNV sensitivity to MβCD followed a similar timecourse (loss of inhibition from 6-8 hpi, Fig 3B-C) suggesting that MβCD also inhibits BUNV early stages of infection. Next, using tris(2-carboxyethyl)phosphine (TCEP) to distinguish between internalized and surface-bound particles, we assessed the kinetics of BUNV cell penetration. TCEP is a membrane-impermeable reducing agent, that unactivates BUNV still exposed extraceullarly or at the plasma membrane. In samples treated with TCEP before warming, we observed a loss of TCEP inhibition after 40 mins of virus addition as assessed by immunofluorescence (Fig. 4D-E) and western blot analysis (Fig. F). Taking into account the NH_4Cl effects on BUNV, we could confirm that BUNV is resident in the endosomal system from 40 min to 6 hrs post-infection. Importantly, an effect of cholesterol depletion on BUNV penetration was discounted as we observed fluorescently-labelled BUNV (BUNV-DiDvbt/SYTO82) in which the viral envelope was labelled with DiDvbt and its RNA genome labelled with SYTO82 in distinct endosomal puncta in cells treated with MβCD, suggesting that BUNV can

penetrate cells depleted of cholesterol (Fig 3D-E). These data suggest that the critical role of cholesterol in the BUNV lifecycle occurs at a post-penetration (≥40 min)/endocytic stage (≤ 6hrs) in agreement with that observed for other enveloped viruses (35).

Cholesterol extraction reduces K^+ accumulation in endosomes

We recently demonstrated that an increasing K^+ gradient is required to induce a fusogenic state in BUNV and HAZV as they traffic through the endocytic network (16, 36), with high [K^+] acting as a biochemical cue for priming/activation of the fusion glycoproteins Gn/Gc (17). Blocking K^+ influx into endosomes was shown to trap virions in the endocytic system, after which they accumulated in lysosomes for subsequent degradation.

Based on this knowledge, and our observation that cholesterol depletion influences BUNV at the stage of endosomal trafficking, we explored whether cholesterol depletion also influences endosomal K^+ accumulation. To test this, we used the K^+-sensitive membrane impermeable fluorescent dye Asante-K^+ green 4 (AG4) that specifically labels endosomal K^+. Endosomes rich in K^+ could be observed within cells in which the intensity of the AG4 signal indicates the degree of K^+ accumulation (Fig 4A-B). When cells were treated with MβCD for 45 minutes and AG4 added, the number of AG4 puncta was reduced compared to 'no-drug' treated cells (Fig 4A-B), suggesting that cholesterol depletion reduces the number of K^+-rich endosomes. Alexa-fluor-594©-conjugated transferrin (TF-594) was used as a control in these experiments to demonstrate no interference of MβCD with general fluorescence or cellular uptake pathways (Fig 4A and 4C). Interestingly, we found that the intensity of TF-594 increased in MβCD-treated cells (2-fold increase) which may be attributed to a shift between recycling and degradation pathways following cholesterol depletion. The above data were confirmed through quantification of the AG4 and TF-594 signals (Figs 4B and C respectively) in which the AG4 signal was reduced to 41.6% and TF-594 increased by 81.6% following MβCD-treatment. These data reveal an important cell biological phenomenon whereby endosomal K^+ accumulation is dependent on cholesterol within endosomal membranes.

To further dissect the relationship between endosomal K^+ and cholesterol we 'primed' BUNV virions for fusion by incubation with K^+ prior to their addition to cells depleted of cholesterol. K^+ priming leads to the activation of the viral fusion machinery, such that endosomal K^+ concentrations no longer influence fusion. If the inhibitory effect of MβCD on infection is a consequence of altering K^+ within endosomes, then this K^+ priming should alleviate the effect of MβCD on virus growth.

To test this, cells were treated with MβCD for 1 hour, whilst virions were incubated for 2 hours in mildly acidic buffers (pH 6.35), with or without exposure to high K^+. Following incubation, the virions were incubated in normal media prior to infection (MOI 0.1) so as to dilute out the high K^+, and return the pH to neutral. Infection was allowed to proceed for 18 hrs, to allow the initiation of BUNV-N production according to our previous time-course analysis (17).

The data in Fig 4D show a significant increase in BUNV-N production when virions are treated in the presence of K^+ (+), compared to without K^+ (-), consistent with our previous studies demonstrating that pH 6.35/K^+ primed virions undergo an accelerated entry stage of their life cycle (16). In cells treated with MβCD, infection was notably decreased for virions incubated without high K^+, consistent with that shown in Fig 1. Critically however, when virions were treated with pH 6.35/high K^+, infection in the presence of MβCD-treatment was almost equivalent to no-drug cells,

suggesting that K^+ primed virions overcome the effects of MβCD and thus do not require cellular cholesterol (Fig. 4D & E). The activity of MβCD in these assays was further confirmed through its known ability to inhibit EGF uptake (Fig. 4F). Taken together, these data imply that the major effects of cholesterol depletion on BUNV are mediated through its effects on cellular endosomal [K^+].

Cellular cholesterol is also required for HAZV infection through its effects on endosomal K^+

BUNV and HAZV are both members of the Bunyavirales order, and their entry pathways have similarities [6,33,34]. We therefore examined whether HAZV, like BUNV, requires cellular cholesterol during entry, thus establishing the possibility of an order-wide dependence.

We first explored if cholesterol depletion similarly impedes HAZV infection using experimental conditions identical to those described for BUNV. Cells were infected with HAZV (MOI 0.2) and the reliance on cholesterol examined through the detection of HAZV-N by either immunofluorescence or western blotting. Following cellular MβCD treatment, a clear decrease in the number of HAZV-infected cells was observed (Fig 5A) which when quantified revealed a 59.47% decrease compared to no-drug controls (Fig 5B, black bars). These data were supported by western blot analysis (Fig 5C) in which HAZV-N expression decreased in a concentration dependent manner with 2 mM MβCD treatment reducing HAZV-N to 78.58% (Fig 5D). The cholesterol requirement of HAZV was further confirmed via treatment of cells with PF-429242 (Fig 5E and F) and U-18666A (Fig 5G and H). Western blot analysis of HAZV-N in PF-429242 treated cells (Fig 5E) revealed a concentration dependent inhibition, which when quantitated showed a decrease in infection to 51.72%, 67.12% and 98.66% in cells treated with 20, 10 and 5 μM PF-429242 respectively (Fig 5F, black bars). When experiments were performed using U18666A, a concentration dependent inhibition of HAZV was also observed (Fig 5G), revealing a reduction of HAZV infection to 22.98% in cells treated with 10 μM U18666A, 35.41% with 5 μM and to 47.52% with 2.5 μM (Fig 5H). MTS data (grey bars in all panels) demonstrated no cellular toxicity in response to any drug treatment. We further sought to explore the effect of the cholesterol requirement of HAZV by using the clinically approved compound simvastatin. Western blot analysis of HAZV-N in simvastatin-treated cells revealed a concentration-dependent inhibition of infection (Fig 5I), which when quantified yielded a reduction of HAZV-N to 44.77%, 59.99%, 67.64% and 85.20% in cells treated with 50, 35, 20 and 10μM respectively.

We have previously shown that high [K^+] activates the fusion machinery of HAZV at pH 7.35 [15]. As such, we sought to explore whether the effect of HAZV 'priming' could also de-sensitise virions to the effects of cholesterol depletion. To test this, cells were treated with MβCD for one hour and HAZV virions were incubated for 2 hours in buffers of pH 7.35 with or without high [K^+]. Virions were subsequently added to normal media to dilute high the [K^+] and added to cells for 18 hours (MOI 0.1).

Fig 5L shows a significant increase in HAZV-N production when primed with high [K^+] (+) at pH 7.35, compared to unprimed virions at pH 7.35 alone (-), suggesting that these conditions expedite an early stage of the HAZV life cycle in a manner comparable to the effect seen in BUNV. Similarly to the effects shown in Fig 4A-D, MβCD-treatment significantly inhibited HAZV infection when treated without high K^+ (-). Importantly, when HAZV virions were primed with high K^+ (+), infection of MβCD-treated cells occurred at levels similar to that of no-drug cells, suggesting that HAZV is also able to overcome the effects of MβCD on cells

when primed with high K^+. These data reinforce the dependence of HAZV on the correct endosomal environment for entry, and further suggest that cholesterol mediates the formation of K^+-rich endosomes required for the escape of BUNV and HAZV virions.

DISCUSSION

The composition of biological membranes is crucial to the physiological function of cells, and cholesterol is an important regulator of membrane integrity and fluidity (18). As such, aberrations in cholesterol homeostasis can disrupt cellular uptake mechanisms, including uptake of both beneficial and detrimental cargos.

By performing pharmacological manipulation of cellular cholesterol content via extraction with MβCD, or interfering with sterol synthesis/trafficking pathways (inhibition using PF-429242, U-18666A and simvastatin), we showed that both BUNV and HAZV are sensitive to changes in cellular cholesterol content (Fig 1 and Fig 5). As such, the peribunyaviruses and nairoviruses can be added to the list of virus families that are known to require cholesterol to establish an infection (37). This list includes many enveloped viruses, for which cholesterol depletion has been reported to disrupt specific stages of the virus life cycle. For example, in the case of the togavirus SFV and influenza virus, cholesterol has a role in membrane fusion (19, 35), whereas in contrast the polyomavirus SV40 requires cholesterol as it enters cells through caveolae-mediated endocytosis (originating from cholesterol rich lipid rafts) (38, 39). In the case of the flavivirus West Nile virus (WNV) cellular cholesterol depletion restricts virus replication as a result of the disruption of cholesterol-rich microdomains (40). The flavivirus hepatitis C virus is also sensitive to changes in cellular cholesterol accumulation (resulting from U-18666A treatment) but the affected stage of the replication cycle is late, namely virus assembly and egress (31). In this study, time of addition experiments and the progression of labelled viruses showed that the effect of cholesterol depletion on BUNV was not at the initial stage of cell penetration, but occurred during the time period when the virus escapes from the endocytic pathway. Furthermore, we showed that cholesterol depletion reduced K^+ accumulation in the endocytic network, leading us to question whether the role of cholesterol in BUNV entry was linked to endosomal K^+ homeostasis, a factor we have shown to be critical for BUNV and HAZV entry (17, 36, 41).

However, a competing possibility was that cholesterol depletion influences membrane fluidity and thus obstructed fusion between viral and endosomal envelopes. To rule out this latter possibility, we 'primed' BUNV by addition of K^+, thus circumventing the need for elevated K^+ in endosomes. Our observation that the entry of primed virus was no longer hindered by cholesterol depletion indicated that restriction of virus growth was not related to membrane fluidity. Instead, we suggest our findings are consistent with cholesterol disrupting K^+ accumulation in endosomes, which consequently hinders activation of the fusion machinery in the appropriate endosomal compartment. One possible mechanism by which this may occur is that the cellular channels responsible for endosomal K^+ accumulation require cholesterol containing membrane sub-domains either for their full activity, or alternatively for incorporation into their native endosomal targets. As such, channels residing in endosomal membranes depleted of cholesterol may show impaired activity, thus slowing or preventing K^+ influx into endosomes, inhibiting the K^+ cue for endosomal escape (Fig. 6). Interestingly, cholesterol can influence K^+ channel functionality and has been found in association with the two-pore domain K^+ (K_{2p}) channels, acting as a linker between the central cavities of these channels and the plasma membrane core (42). Work is in

progress in our laboratory to identify the specific cellular K^+ channel(s) involved in endosomal K^+ accumulation, and current evidence derived from an extensive pharmacological screen of blocking agents indicates it is a member of the above mentioned K_{2P} channel family. Once this information is confirmed, we will be able to further our current findings by examining how cholesterol influences the distribution or activity of the K_{2P} channel involved.

While our findings reported here represent the first identification of a cholesterol requirement for infection by members of either the Peribunyaviridae or Nairoviridae families, a previous study revealed that replication of Andes virus (ANDV), a pathogenic hantavirus of the Bunyavirales order was blocked when the major cellular sterol pathway was dysregulated either by genetic or pharmacological means(20). Critical genes involved included SREBP2, S1P, S2P and SCAP, and gene ablation or knock-down studies using a non-replicating recombinant vesicular stomatitis virus pseudotyped with ANDV-G revealed a block in an undetermined stage of entry. The sterol pathway requirement was extended to infectious ANDV, and treatment of cells with a statin (mevastatin), a clinically-approved cholesterol lowering drug, reduced infection by over 10-fold. Despite the fundamental differences between hantaviruses, peribunyaviruses and nairoviruses that has led to their taxonomic separation, the possibility that infection and disease caused by highly pathogenic bunyaviruses may be treated or prevented by treatment with existing drugs is an exciting prospect.

EXPERIMENTAL PROCEDURES

Cells and Virus

A549 (lung epithelial carcinoma) and SW13 (human adrenal carcinoma) cells were obtained from the European Collection of Cell Cultures (ECACC). A549 and SW13 cells were maintained in a humidified incubator at 37°C with 5% CO_2, and cultured in Dulbecco's modified eagle's medium (DMEM, Sigma-Aldrich) with 10% foetal calf serum (FCS), 100 U/ml penicillin and 100 µg/ml streptomycin (1% pen/strep). For the experiments detailed below, unless otherwise specified, A549 and SW13 cells were seeded into 6 well (~$0.3x10^6$ cells/well) or 12 well plates (~$0.1x10^6$ cells/well) and incubated at 37ºC for 24 hrs to allow cell adherence prior to each experiment.

Wild-type BUNV and HAZV stocks were made from clarified baby hamster kidney (BHK) cell supernatants and stored at -80°C, suspended in DMEM and 10% FCS. Titres were estimated by plaque assay, yielding ~$3.5x10^6$ PFU/ml and ~$7x10^6$ PFU/ml for BUNV and HAZV respectively.

SYTO82/DiD-labelled BUNV was produced as described previously (16), whereby the three RNA segments are labelled using a SYTO82 nucleic acid stain, the viral lipid envelope labelled using a DiD-vybrant lipid label and the virions purified. Recombinant BUNV in which eGFP is fused to the N terminus of truncated Gc (BUNV-GFP) was kindly provided by Xiaohong Shi from CVR Glasgow).

Virus Infection & Drug Treatment Assays

TCEP Assays

Stock solutions of Tris (2-carboxyethyl) phosphine hydrochloride (TCEP, Sigma-Aldrich) were made to 1 M in deionised sterile water and frozen at -20°C. These stocks were diluted to 10 mM in Opti-MEM reduced serum media (Gibco) prior to each experiment. A549 cells were infected with BUNV or HAZV (MOI = 0.2) (T=0) and incubated at 37°C. Cells were washed in phosphate-buffered saline (PBS) and 10 mM TCEP added for 5 minutes at the time points indicated; 0.5-120 minutes post infection. Cells were washed in PBS following TCEP treatments and incubated at 37°C in DMEM. Cells were lysed or fixed at 24 hpi and immunoblotted or immunostained (see below) for IncuCyte Zoom® analysis of viral N protein.

MβCD Entry Assays

A549 cells were PBS washed and pre-infection treated with 2 mM, 1 mM or 0.5 mM methyl-beta cyclodextrin (MβCD, Sigma-Aldrich) for 45 minutes at 37°C. Cells were PBS washed to remove drug and infected with BUNV or HAZV (MOI = 0.2) for 2 hours to allow virus entry. Media and non-internalised virions were removed via 1xPBS wash and 3x 0.5% trypsin washes (2 hpi) and replaced with complete DMEM. Infection was allowed to proceed until 24 hpi, followed by lysis or fixation for western blot or IncuCyte Zoom® analysis.

Simvastatin, PF-429242 and U18666A Entry Assays

A549 cells were treated with Simvastatin (Sigma-Aldrich; 10, 20, 25 or 50 µM), PF-429242 (Sigma-Aldrich; 20, 10 or 5 µM) or U-18666A (Abcam; 10, 5 or 2.5 µM) for 24 hours. Cells were subsequently infected with BUNV or HAZV (MOI = 0.2) for 24 hours with the drug(s) maintained throughout. At 24 hpi cells were lysed for analysis.

SYTO82/DiD-labelled BUNV infection of *MβCD*-treated cells

A549 cells were seeded onto 1 cm^2 glass-bottom 8-well µ-slides (Ibidi). Cells were treated with 2 mM MβCD for 45 minutes, after which drug was washed off with PBS and cells infected with SYTO82/DiD-labelled BUNV (MOI = ~8) for 30 minutes at 4°C, to allow virus binding. This was followed by warming to 37°C, to allow synchronised entry, and incubation for 8 hours. 30 minutes prior to

imaging cells were stained with CytoPainter organelle stain (Abcam) for 30 minutes. Cells were washed with PBS and live imaged by confocal microscopy in fresh DMEM.

*MβCD and NH_4*Cl Time of Addition Assays

A549 cells (x8 wells total) were infected with BUNV (MOI (0.1) (t=0), with one well pre-treated (0 hpi time point) with MβCD (2 mM) or ammonium chloride (NH_4Cl, 10 mM, Sigma-Aldrich) for 45 minutes prior to infection. At 1 hpi non-internalised virus was washed off and media or drug added to the corresponding wells. MβCD or NH_4Cl was added to cells at the time points indicated; 1-10 hpi. Infection was allowed to proceed until 24 hpi, lysed and BUNV infection assessed by western blot detection of BUNV-N.

Viral Envelope Cholesterol Depletion

HAZV or BUNV-GFP virions were treated with MβCD (2 mM) for 90 minutes at 37°C. MβCD was diluted into complete media and A549 cells were subsequently infected with treated virions (MOI 0.5) for 24 hours. Cells were fixed or lysed for the detection of HAZV-N/GFP by immunofluorescent staining (IncuCyte Zoom®) or HAZV-N/BUNV-N by western blotting.

Visualisation of MβCD-treated BUNV by negative staining

BUNV was collected from BHK-21 supernatants, purified through 30% sucrose and re-suspended overnight in 0.1x PBS. Purified BUNV virions ($1.5x10^9$ PFU/ml) were treated with 2 mM MβCD for 90 minutes at 37°C. Preparations were added to glow-discharged carbon-coated grids and allowed to stand for 1 minute. Grids were washed 3x with dH_20 and stained for 1 minute with 1% aqueous uranyl acetate. Preparations were allowed to dry and imaged using a FEI Tecnai T12 electron microscope at 120 kV. Images were collected at a nominal defocus between -1 and -5 µm using a Gatan Ultrascan 4000 CCD camera.

BUNV/HAZV Priming Recovery Assays

BUNV virions (12 µl; MOI 0.1) were diluted 1:11 in buffers mimicking the change in endosomal pH (pH 7.35 or 6.35) and K^+ concentration (0 or 140 mM KCl), and incubated for 2 hours at 37°C). Buffers were diluted out into 2 ml fresh DMEM prior to addition onto cells and added immediately to A549 cells. For the MβCD (2 mM) drug-treated samples, cells were treated for 1 hour prior to infection (during virus priming) or left untreated, and drug was removed from wells prior to infection. Cells were incubated until 18 hpi and lysed. HAZV virions (24µl; MOI 0.1) were diluted 1:11 in buffers mimicking early endosomal compartments (pH 7.35) plus or minus 140 mM KCl, and incubated as above. A549 cells were treated with 2 mM MβCD for 1 hour during priming or left untreated so as to mirror the conditions used in BUNV assays, and infected with HAZV/buffer in 2ml fresh DMEM for 18 hours prior to lysis and screening for HAZV-N.

pH/ion Buffer Preparation

A pH 7.35 buffer was used as a control alongside pH 6.35 buffers with a high or low K^+ concentration, prepared with 0.2 M Tris (pH 7.35) or 0.3 M Bis-Tris (pH 6.35). The desired salt concentrations were achieved by adding 12 mM NaCl and +/- 140 mM KCl. On the day of use buffers were adjusted to desired temperature and pH using 30% HCl.

K^+ Uptake Assays

A549 cells were treated pre-infection with 2 mM MβCD in Opti-MEM for 45 minutes at 37°C, or left untreated as a control. Cells were simultaneously treated with 10 µM membrane-impermeable Asante Potassium Green-4 (AG4) and 2 µg/ml Alexa Fluor-conjugated Transferrin-594 for 45 minutes, with MβCD in the media throughout. Cells were washed in

PBS and live imaged using the IncuCyte Zoom® system.

MTS Cell Viability Assays

A549 cells were seeded into 96-well tissue culture plates ($0.05x10^6$ cells/well) and allowed to grow to 70-80% confluency. Cells were then treated with the respective drugs alongside an untreated and H_2O treated control for 24 hours, the maximum time these drugs were applied for. Cells were then screened for viability using CellTitre 96® reagent (Promega), 20 µl added in serum free media following manufacturer's instructions for 1 hour. Viability was analysed by reading absorbance at 570 nm using a plate reader. Results were normalised to the untreated control.

Western Blot Analysis

At the time points stated cells were lysed in Leeds Lysis Buffer (LLB; 25 mM glycerol phosphate, 20 mM tris, 150 mM NaCl, 1 mM EDTA, 1% triton x 100, 10% glycerol, 50 mM NaF, 5 mM $Na_4O_7P_2$, pH 7.4) plus protease inhibitor cocktail (Thermo Scientific) for 15 minutes at 4°C. Lysates were resolved on 12% or 15% sodium-dodecyl sulphate (SDS) gels using SDS-PAGE. Protein was transferred onto polyvinylidene difluoride (PVDF; Millipore) membranes using a Bio-Rad Trans-blot Turbo. Membranes were blocked in 10% milk in TBS-tween for 1 hour. Proteins were labelled with primary antibodies in 5% milk in TBS-tween for 1 hour at room temperature, then with corresponding HRP-conjugated secondary antibodies in 5% milk/TBS-tween. Labelled proteins were detected by enhanced chemiluminescence (ECL) and film developed using an Xograph processor. Quantification of bands was performed using densitometry on ImageJ software.

BUNV/HAZV was detected using BUNV-N/HAZV-N primary antibodies and corresponding anti-sheep secondary antibodies (1:5000). Anti-GAPDH antibodies were used as a loading control alongside anti-mouse secondary antibodies (1:5000).

Immunofluorescence Staining

Confocal Analysis

Cells were live imaged using an inverted LSM-880 confocal microscope (Zeiss) on an oil-immersion 63x objective lens to image fluorescent labelling - SYTO82 ($em._{max}$ 560 nm), DiDvbt ($em._{max}$ 665 nm), conjugated transferrin-488 ($em._{max}$ 518 nm).

IncuCyte Analysis

At the indicated time points, cells were fixed in 4% paraformaldehyde for 10 minutes at 4°C. Cells were PBS washed and permeabilised with cold 50% methanol/acetone for 10 minutes at 4°C. Non-specific antibody binding was then blocked with 1% bovine serum albumin (BSA) in PBS at room temperature for 15 minutes. Primary anti-BUNV-N or HAZV-N antibodies were added (1:5000) in 1% BSA for 1 hour, followed by 4x PBS washes. Corresponding fluorescent Alexa-Fluor®-594 conjugated anti-sheep (Invitrogen-Molecular Probes) secondary antibodies (1:500) were added for 2 hours in 1% BSA, followed by 4x washes in PBS. For K^+ uptake assays (2.2.8) cells were live imaged, without fixing of staining protocols outlined above.

Cells were imaged using the IncuCyte Zoom® system, widefield images of 2.15 mm^2 were taken and fluorescently-labelled infected cells could be identified. The mean fluorescence count per well was quantified for treated cells using the IncuCyte Zoom® 2018 software and results normalised to those of untreated cells.

Acknowledgements
JM is funded by a Royal Society Fellowship (RG110306 & UF100419). JM and JF are funded by the Academic Fellow scheme at the University of Leeds. The FEI Tecnai G^2-Spirit was funded by The Wellcome Trust (090932/Z/09/Z). The funders had no role in study design, data collection and analysis, decision to publish, or preparation of the manuscript. We thank Xiaohong Shi (CVR Glasgow) for the kind gift of the GFP-BUNV.

Conflict of interest
The authors declare that they have no conflicts of interest with the contents of this article.

Figure Legends

Figure 1. BUNV infection is inhibited by cellular cholesterol depletion. (A). A549 cells were treated with MβCD for 45 minutes and infected with BUNV (MOI 0.2). At 24 hpi cells were fixed and stained for BUNV-N. Widefield images were taken using an IncuCyte ZOOM® (representative images are shown). (B) The percentage of BUNV infected cells was quantified using IncuCyte Zoom® software and normalised to no-drug cells (black bars) (*$p<0.05$, error bars representative of ±SD, n=3). Cell viability was assessed by MTS assays. Values were normalised to no-drug cells (grey bars). (C) Entry assays were performed as in (A), cell lysates were resolved via SDS-PAGE, and BUNV-N expression was assessed by western blot analysis. GAPDH was probed as a loading control. (D) Densitometry analysis of (C). Band densities were normalised to no-drug BUNV infected cells (black bars). MTS cell viability data is also shown (grey bars). (E) BUNV entry assays were performed in the presence of PF-429242. Cells were treated with 5-20 μM PF-429242 for 24 hours and infected with BUNV (MOI 0.2) for a further 24 hrs. Cells were lysed, and lysates were resolved via SDS-PAGE and screened for BUNV-N and GAPDH. (F) Densitometry analysis of (E). (G) Entry assays performed as in (E) with U-18666A at 2.5-10 μM. (H) Densitometry analysis of BUNV-N expression following U-18666A treatment. (I) Entry assays as in (E) with 10-50 μM Simvastatin. (J) Densitometry analysis of (I) as in (D).

Figure 2. BUNV envelope cholesterol is also required for virus infection. (A) Schematic of BUNV envelope cholesterol extraction. GFP-BUNV virions were treated with MßCD for 90 minutes and the drug/virus was diluted in DMEM and added to A549 cells for 24 hours (MOI 0.5). (B) Cells were lysed and BUNV-N expression was assessed by western blot analysis. (C) Blots were quantified by densitometry analysis and normalised to no drug controls (*$p<0.05$, error bars ± SD, n=3) (D) Virions were treated as in (A) and GFP expression, as a marker of BUNV infection, was assessed by IncuCyte analysis. Representative widefield images are shown. (E) Percentage of cells infected by MßCD-treated virions were measured using IncuCyte ZOOM® software (*$p<0.05$; error bars ±SD, n=3). (F) Purified BUNV virions were treated with 2 mM MβCD for 90 minutes at 37°C. Treated and untreated (no-drug) virions were loaded onto carbon-coated grids and negatively-stained with 1% uranyl acetate. Images were taken at 120 kV on a Tecnai T12 electron microscope.

Figure 3. MβCD inhibits BUNV at an early post-penetration stage of infection. (A) A549 cells were infected with BUNV (MOI 0.1) (t=0). NH_4Cl was added at the indicated time points and screened for BUNV-N expression at 24 hpi by western blot as in Fig.1. (B) Cells were infected and treated with MβCD as in (A). (C). Densitometry analysis of NH_4Cl and MβCD time courses (A) and (B) (grey and black bars respectively). Band densities were normalised to no-drug infected cells (*$p<0.05$, NS = non-significant, error bars ±SD, n=3). BUNV internalisation

takes up to 40 minutes. (D) BUNV virions were added to A549 cells (MOI 0.2) (t=0), which were treated with the cell impermeable reducing agent Tris (2-carboxyethyl) phosphine hydrochloride (TCEP) for 5 minutes at the indicated post-infection time points (20-120 minutes). Cells were fixed at 24 hpi, stained for BUNV-N and widefield images were taken using the IncuCyte ZOOM®. (E) The percentage of infected cells was quantified using IncuCyte Zoom® software. Values are normalised to no-drug infected cells (*$p<0.05$, NS = non-significant, error bars ±SD, n=3). (F) TCEP assays were performed as in (D) and cell lysates were harvested and resolved via SDS-PAGE. Lysates were screened for BUNV-N by western blot analysis. GAPDH was probed as a loading control. (G) No-drug treated A549 cells were infected with SYTO82/DiD-BUNV (MOI ~8) for 8 hours at 37°C. Cytopainter was added 30 minutes prior to live imaging as a cell marker (scale bar 10 µm. Fluorescent BUNV stained with SYTO82 (em.max 560 nm) and DiDvbt (em.max 665 nm) were imaged alongside cytopainter (em.max 488 nm). (H) Cells were pre-treated with MßCD for 45 minutes prior to infection with SYTO82/DiD-BUNV as in (D). Representative confocal images are shown (Scale bar 10 µM).

Figure 4. MβCD inhibits endosomal K^+ accumulation, whilst K^+ primed BUNV virions can overcome cellular cholesterol depletion. (A) Cells were pre-treated with MβCD (or no-drug control) for 45 minutes and the cell-impermeable K^+ dye Asante Potassium Green-4 (AG4) and Transferrin-594 (TF-594) were added for 45 minutes at 37°C to permit endosomal uptake. Non-internalised dyes were removed through PBS washes and live cells were imaged using the IncuCyte ZOOM®. Representative widefield images are shown (B) AG4 fluorescence was quantified in MβCD-treated cells and normalised to no-drug cells (*$p<0.05$, NS = non-significant, error bars ±SD, n=3). (C) Quantitative analysis of TF-594 internalisation in no-drug vs MβCD-treated cells, analysed as in (B). (D) Cells were pre-treated with MβCD for 1 hr and BUNV virions were treated with buffers at pH 6.35, with or without 140 mM KCl, for 2 hours at 37°C. Buffers were diluted into 2 ml of fresh DMEM and immediately added to A549 cells. Cells were lysed 18 hpi and immunoblotted for BUNV-N as in Fig 1C. (E) Densitometry analysis of (D) as in Fig 1D. (F) Cells were pre-treated with 0.5, 1 or 2 mM MßCD for 45 minutes and 2 µg/ml EGF-488 was added to cells for 30 minutes. Widefield images were taken using IncuCyte Zoom ® software.

Figure 5. HAZV infection is also inhibited by cellular cholesterol depletion. (A) A549 cells were treated with MβCD for 45 minutes and infected with HAZV (MOI 0.2). Cells were fixed at 24 hpi and stained for HAZV-N. Widefield images were obtained using the IncuCyte ZOOM®. (B) The % of infected cells was quantified using IncuCyte Zoom® software, and normalised to no-drug cells (black bars; *$p<0.05$, error bars ± SD, n=3). Cell viability was assessed by MTS assay and normalised to no-drug cells (grey bars). (C) Entry assays were performed as in (A), cells were lysed and HAZV-N expression was assessed by western blot analysis. GAPDH was used as a control to confirm equal protein loading. (D) Densitometry analysis of (C). Band densities were normalised to no-drug cells (black bars, NS = non-significant, n=3) and compared to MTS cell viability data (grey bars). (E) HAZV entry assays in the presence of PF-429242. Cells were pre-treated with 5-20 µM PF-429242 for 24 hours and infected with HAZV (MOI 0.2). Cells were lysed at 24 hpi and screened for HAZV-N and GAPDH as in (C). (F) Densitometry analysis of (E) as in (D). (G) Entry assays performed as in (E) with U-18666A at 2.5-10 µM. (H) Densitometry analysis of (G) as in (D). (I) HAZV entry assays were performed in the presence of simvastatin. Cells were pre-treated with 10-50 µM simvastatin for 24 hours and infected with HAZV (MOI 0.2). Cells were lysed and screened for HAZV-N and GAPDH as in (C). (J) Densitometry analysis of (I) as in (D). (K) Cells were pre-treated with MβCD for one hour. Simultaneously, HAZV virions were treated with buffers

at pH 7.35 with or without 140 mM KCl, for 2 hours at 37°C. The buffers were diluted out into 2 ml of DMEM and immediately added to A549 cells. Cells were lysed at 18 hpi and immunoblotted for HAZV-N as in Fig 1C. (L) Densitometry analysis of (K) as in Fig 1D. (H)

Figure 6. Cholesterol depletion may perturb K^+ accumulation in endosomes, preventing virus escape. A putative model for the potential role of cholesterol in the accumulation of endosomal K^+ ions. (A) Endosomal pH and the K^+ gradient provides the biochemical cue for virus fusion and endosomal escape. This process is likely to be mediated by endosomal K^+ channels. (B) Cholesterol depletion may inactivate or impair the function of the K^+ channel(s) in endosomal membranes, slowing or preventing K^+ influx into BUNV-containing endosomes. As such, BUNV is able to penetrate cells and be internalised into endosomes, but the K^+ cue is inhibited, impairing endosomal escape and subsequent virus infection.

REFERENCES

1. Wolf, Y; Krupovic, M; Zhang, Y Z; Maes, P; Dolja, V; Koonin, E V; Kuhn, J. (2018) Megataxonomy of negative-sense RNA viruses. Int. Comm. Taxon. Viruses. [online] https://talk.ictvonline.org/taxonomy/ (Accessed January 17, 2019)

2. Soldan, S. S., and González-Scarano, F. (2005) Emerging infectious diseases: The Bunyaviridae. J. Neurovirol. **11**, 412–423

3. Elliott, R. M. (1997) Emerging viruses: the Bunyaviridae. Mol. Med. **3**, 572–7

4. Simons, J. F., Hellman, U., and Pettersson, R. F. (1990) Uukuniemi virus S RNA segment: ambisense coding strategy, packaging of complementary strands into virions, and homology to members of the genus Phlebovirus. J. Virol. **64**, 247–55

5. Fuller, F., Bhown, A. S., and Bishop, D. H. L. (1983) Bunyavirus Nucleoprotein, N, and a Non-structural Protein, NSS, Are Coded by Overlapping Reading Frames in the S RNA. J. Gen. Virol. **64**, 1705–1714

6. Vera-Otarola, J., Solis, L., Soto-Rifo, R., Ricci, E. P., Pino, K., Tischler, N. D., Ohlmann, T., Darlix, J.-L., and López-Lastra, M. (2012) The Andes Hantavirus NSs Protein Is Expressed from the Viral Small mRNA by a Leaky Scanning Mechanism. 10.1128/JVI.06223-11

7. Simon, M., Johansson, C., and Mirazimi, A. (2009) Crimean-Congo hemorrhagic fever virus entry and replication is clathrin-, pH- and cholesterol-dependent. J. Gen. Virol. **90**, 210–215

8. Jin, M., Park, J., Lee, S., Park, B., Shin, J., Song, K.-J., Ahn, T.-I., Hwang, S.-Y., Ahn, B.-Y., and Ahn, K. (2002) Hantaan Virus Enters Cells by Clathrin-Dependent Receptor-Mediated Endocytosis. Virology. **294**, 60–69

9. Hollidge, B. S., Nedelsky, N. B., Salzano, M.-V., Fraser, J. W., González-Scarano, F., and Soldan, S. S. (2012) Orthobunyavirus entry into neurons and other mammalian cells occurs via clathrin-mediated endocytosis and requires trafficking into early endosomes. J. Virol. **86**, 7988–8001

10. Lozach, P.-Y., Mancini, R., Bitto, D., Meier, R., Oestereich, L., Överby, A. K., Pettersson, R. F., and Helenius, A. (2010) Entry of Bunyaviruses into Mammalian

Cells. Cell Host Microbe. **7**, 488–499

11. Garry, C. E., and Garry, R. F. (2004) Proteomics computational analyses suggest that the carboxyl terminal glycoproteins of Bunyaviruses are class II viral fusion protein (beta-penetrenes). Theor. Biol. Med. Model. **1**, 10

12. Kuhn, R. J., Zhang, W., Rossmann, M. G., Pletnev, S. V, Corver, J., Lenches, E., Jones, C. T., Mukhopadhyay, S., Chipman, P. R., Strauss, E. G., Baker, T. S., and Strauss, J. H. (2002) Structure of dengue virus: implications for flavivirus organization, maturation, and fusion. Cell. **108**, 717–25

13. von Bonsdorff, C. H., and Pettersson, R. (1975) Surface structure of Uukuniemi virus. J. Virol. **16**, 1296–307

14. von Bonsdorff, C. H., and Harrison, S. C. (1975) Sindbis virus glycoproteins form a regular icosahedral surface lattice. J. Virol. **16**, 141–5

15. Harrison, S. C. (2015) Viral membrane fusion. Virology. **479**–**480**, 498–507

16. Hover, S., Foster, B., Fontana, J., Kohl, A., Goldstein, S. A. N., Barr, J. N., and Mankouri, J. (2018) Bunyavirus requirement for endosomal K+ reveals new roles of cellular ion channels during infection. PLOS Pathog. **14**, e1006845

17. Punch, E. K., Hover, S., Blest, H. T. W., Fuller, J., Hewson, R., Fontana, J., Mankouri, J., and Barr, J. N. (2018) Potassium is a trigger for conformational change in the fusion spike of an enveloped RNA virus. J. Biol. Chem. **293**, 9937–9944

18. Song, Y., Kenworthy, A. K., and Sanders, C. R. (2014) Cholesterol as a co-solvent and a ligand for membrane proteins. Protein Sci. **23**, 1–22

19. Phalen, T., and Kielian, M. (1991) Cholesterol is required for infection by Semliki Forest virus. J. Cell Biol. **112**, 615–23

20. Kleinfelter, L. M., Jangra, R. K., Jae, L. T., Herbert, A. S., Mittler, E., Stiles, K. M., Wirchnianski, A. S., Kielian, M., Brummelkamp, T. R., Dye, J. M., and Chandran, K. (2015) Haploid Genetic Screen Reveals a Profound and Direct Dependence on Cholesterol for Hantavirus Membrane Fusion. MBio. **6**, e00801

21. Chlanda, P., Mekhedov, E., Waters, H., Schwartz, C. L., Fischer, E. R., Ryham, R. J., Cohen, F. S., Blank, P. S., and Zimmerberg, J. (2016) The hemifusion structure induced by influenza virus haemagglutinin is determined by physical properties of the target membranes. Nat. Microbiol. **1**, 16050

22. Bajimaya, S., Frankl, T., Hayashi, T., and Takimoto, T. (2017) Cholesterol is required for stability and infectivity of influenza A and respiratory syncytial viruses. Virology. **510**, 234–241

23. White, J. M., and Whittaker, G. R. (2016) Fusion of Enveloped Viruses in Endosomes. Traffic. **17**, 593–614

24. Cooper, R. A. (1978) Influence of increased membrane cholesterol on membrane fluidity and cell function in human red blood cells. J. Supramol. Struct. **8**, 413–430

25. Hawkins, J. L., Robbins, M. D., Warren, L. C., Xia, D., Petras, S. F., Valentine, J. J.,

Varghese, A. H., Wang, I.-K., Subashi, T. A., Shelly, L. D., Hay, B. A., Landschulz, K. T., Geoghegan, K. F., and Harwood, H. J. (2008) Pharmacologic Inhibition of Site 1 Protease Activity Inhibits Sterol Regulatory Element-Binding Protein Processing and Reduces Lipogenic Enzyme Gene Expression and Lipid Synthesis in Cultured Cells and Experimental Animals. J. Pharmacol. Exp. Ther. **326**, 801–808

26. Cenedella, R. J. (2009) Cholesterol Synthesis Inhibitor U18666A and the Role of Sterol Metabolism and Trafficking in Numerous Pathophysiological Processes. Lipids. **44**, 477–487

27. Petersen, J., Drake, M. J., Bruce, E. A., Riblett, A. M., Didigu, C. A., Wilen, C. B., Malani, N., Male, F., Lee, F.-H., Bushman, F. D., Cherry, S., Doms, R. W., Bates, P., and Briley, K. (2014) The Major Cellular Sterol Regulatory Pathway Is Required for Andes Virus Infection. PLoS Pathog. **10**, e1003911

28. Poh, M. K., Shui, G., Xie, X., Shi, P.-Y., Wenk, M. R., and Gu, F. (2012) U18666A, an intra-cellular cholesterol transport inhibitor, inhibits dengue virus entry and replication. Antiviral Res. **93**, 191–198

29. Wichit, S., Hamel, R., Bernard, E., Talignani, L., Diop, F., Ferraris, P., Liegeois, F., Ekchariyawat, P., Luplertlop, N., Surasombatpattana, P., Thomas, F., Merits, A., Choumet, V., Roques, P., Yssel, H., Briant, L., and Missé, D. (2017) Imipramine Inhibits Chikungunya Virus Replication in Human Skin Fibroblasts through Interference with Intracellular Cholesterol Trafficking. Sci. Rep. **7**, 3145

30. Côté, M., Misasi, J., Ren, T., Bruchez, A., Lee, K., Filone, C. M., Hensley, L., Li, Q., Ory, D., Chandran, K., and Cunningham, J. (2011) Small molecule inhibitors reveal Niemann-Pick C1 is essential for Ebola virus infection. Nature. **477**, 344–8

31. Elgner, F., Ren, H., Medvedev, R., Ploen, D., Himmelsbach, K., Boller, K., and Hildt, E. (2016) The Intracellular Cholesterol Transport Inhibitor U18666A Inhibits the Exosome-Dependent Release of Mature Hepatitis C Virus. J. Virol. **90**, 11181–11196

32. Shi, X., van Mierlo, J. T., French, A., and Elliott, R. M. (2010) Visualizing the replication cycle of bunyamwera orthobunyavirus expressing fluorescent protein-tagged Gc glycoprotein. J. Virol. **84**, 8460–9

33. Shi, X., Goli, J., Clark, G., Brauburger, K., and Elliott, R. M. (2009) Functional analysis of the Bunyamwera orthobunyavirus Gc glycoprotein. J. Gen. Virol. **90**, 2483–92

34. Shi, X., van Mierlo, J. T., French, A., and Elliott, R. M. (2010) Visualizing the replication cycle of bunyamwera orthobunyavirus expressing fluorescent protein-tagged Gc glycoprotein. J. Virol. **84**, 8460–9

35. Sun, X., and Whittaker, G. R. (2003) Role for influenza virus envelope cholesterol in virus entry and infection. J. Virol. **77**, 12543–51

36. Hover, S., King, B., Hall, B., Loundras, E.-A., Taqi, H., Daly, J., Dallas, M., Peers, C., Schnettler, E., McKimmie, C., Kohl, A., Barr, J. N., and Mankouri, J. (2016) Modulation of Potassium Channels Inhibits Bunyavirus Infection. J. Biol. Chem. **291**, 3411–22

37. Kielian, M. C., and Helenius, A. (1984) Role of cholesterol in fusion of Semliki Forest virus with membranes. J. Virol. **52**, 281–3

38. Pelkmans, L., and Helenius, A. (2002) Endocytosis via caveolae. Traffic. **3**, 311–20

39. Pelkmans, L., Kartenbeck, J., and Helenius, A. (2001) Caveolar endocytosis of simian virus 40 reveals a new two-step vesicular-transport pathway to the ER. Nat. Cell Biol. **3**, 473–483

40. Medigeshi, G. R., Hirsch, A. J., Streblow, D. N., Nikolich-Zugich, J., and Nelson, J. A. (2008) West Nile virus entry requires cholesterol-rich membrane microdomains and is independent of alphavbeta3 integrin. J. Virol. **82**, 5212–9

41. Hover, S., Foster, B., Barr, J. N., and Mankouri, J. (2017) Viral dependence on cellular ion channels – an emerging anti-viral target? J. Gen. Virol. **98**, 345–351

42. Lee, A. G. (2018) A Database of Predicted Binding Sites for Cholesterol on Membrane Proteins, Deep in the Membrane. Biophys. J. 10.1016/J.BPJ.2018.06.022

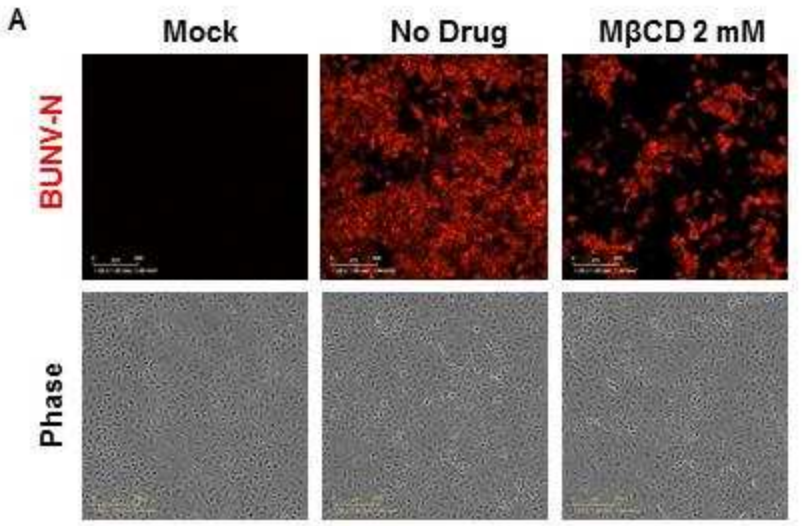
A
Mock
No Drug
MβCD 2 mM
BUNV-N
Phase

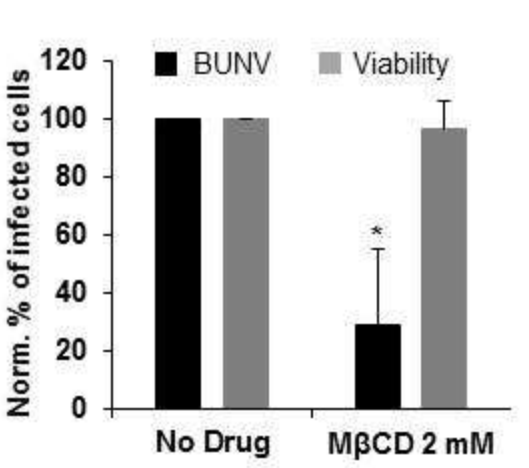
B
BUNV
Viability
Norm. % of infected cells
120
100
80
60
40
20
0
*
No Drug
MβCD 2 mM

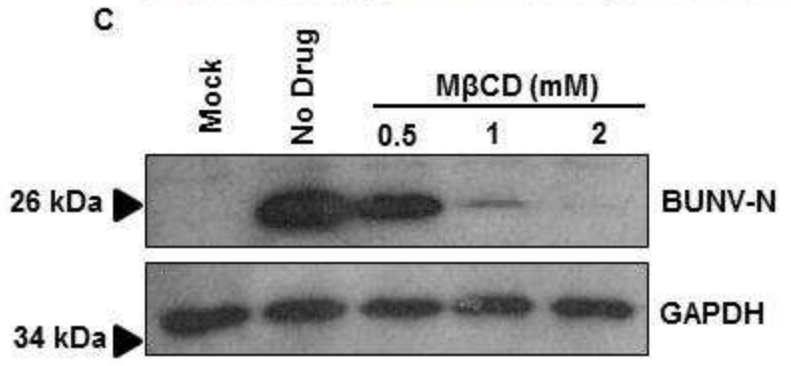
C
Mock
No Drug
MβCD (mM)
0.5
1
2
26 kDa
BUNV-N
34 kDa
GAPDH

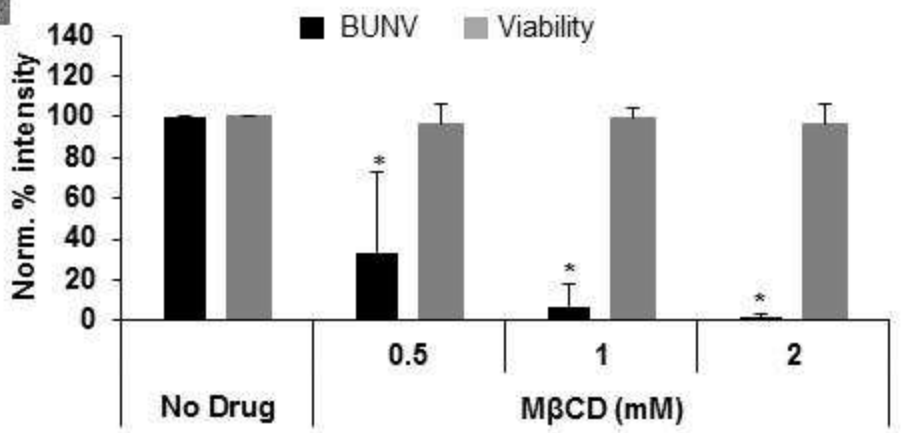
D
BUNV
Viability
Norm. % intensity
140
120
100
80
60
40
20
0
*
No Drug
0.5
1
2
MβCD (mM)

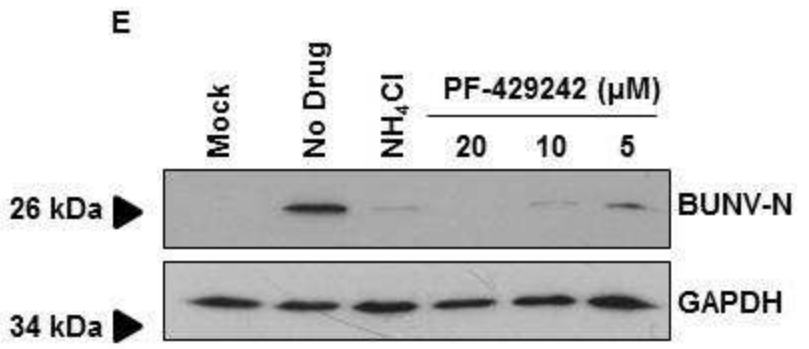
E
Mock
No Drug
NH4Cl
PF-429242 (μM)
20
10
5
26 kDa
BUNV-N
34 kDa
GAPDH

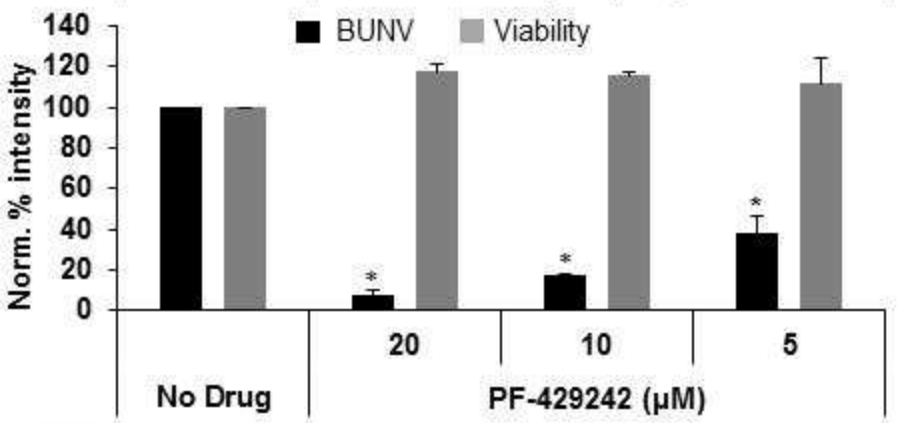
F
BUNV
Viability
Norm. % intensity
140
120
100
80
60
40
20
0
*
No Drug
20
10
5
PF-429242 (μM)

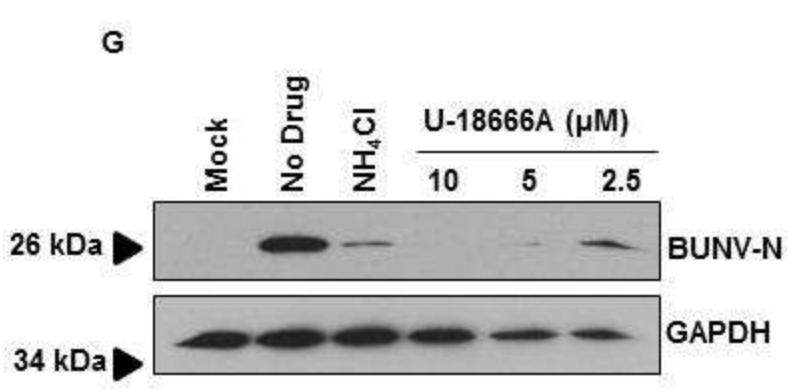
G
Mock
No Drug
NH4Cl
U-18666A (μM)
10
5
2.5
26 kDa
BUNV-N
34 kDa
GAPDH

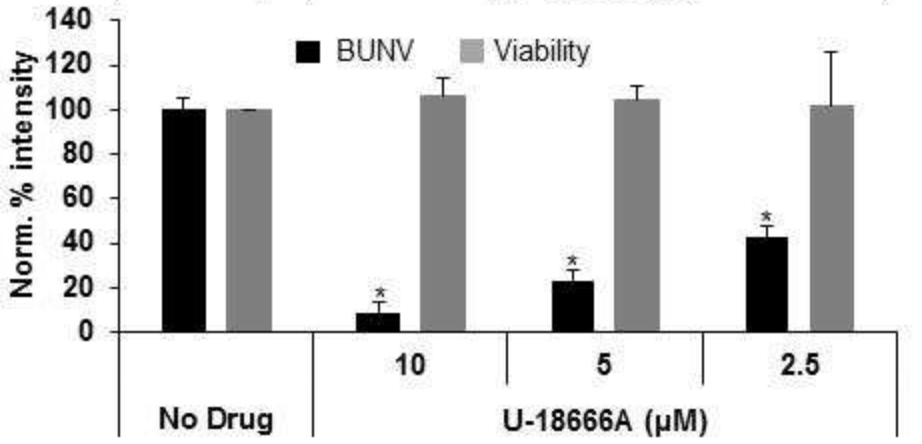
H
BUNV
Viability
Norm. % intensity
140
120
100
80
60
40
20
0
*
No Drug
10
5
2.5
U-18666A (μM)

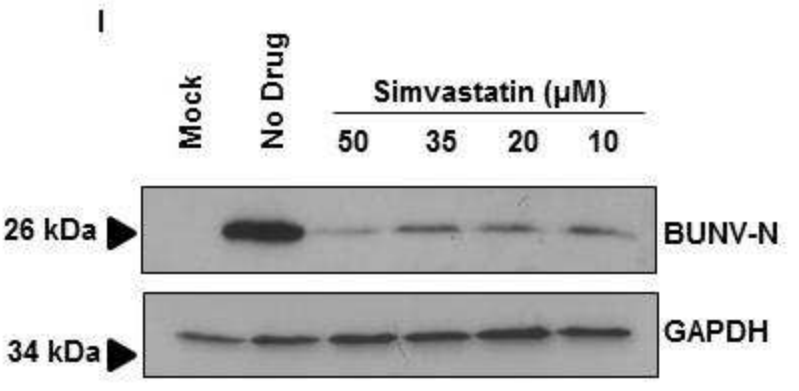
I
Mock
No Drug
Simvastatin (μM)
50
35
20
10
26 kDa
BUNV-N
34 kDa
GAPDH

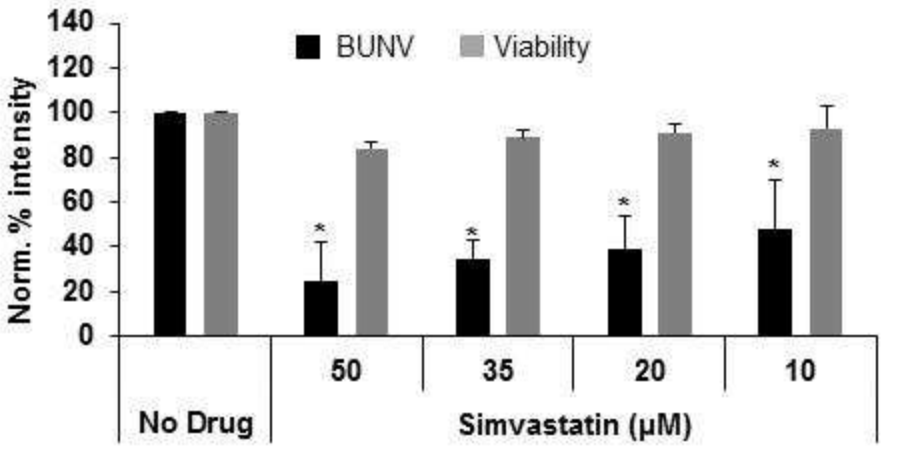
J
BUNV
Viability
Norm. % intensity
140
120
100
80
60
40
20
0
*
No Drug
50
35
20
10
Simvastatin (μM)

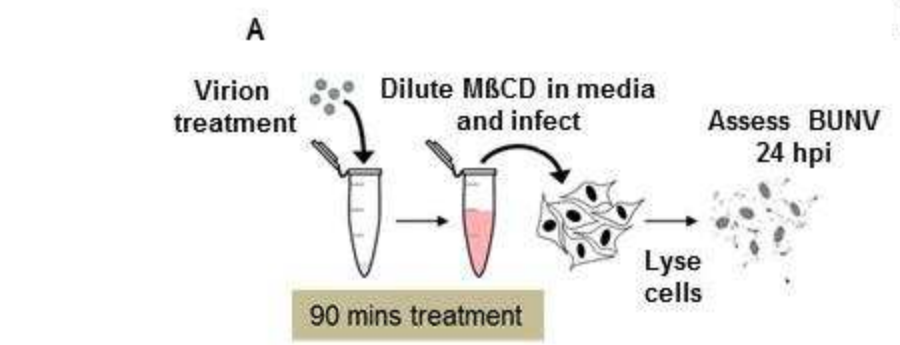
A
Virion treatment
Dilute MßCD in media and infect
Assess BUNV 24 hpi
Lyse cells
90 mins treatment

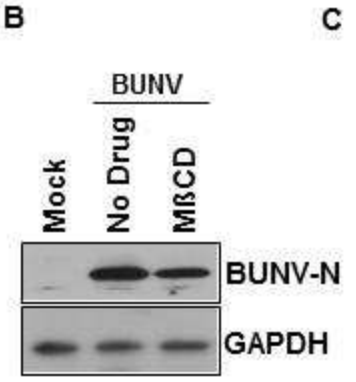
B
BUNV
Mock
No Drug
MßCD
BUNV-N
GAPDH

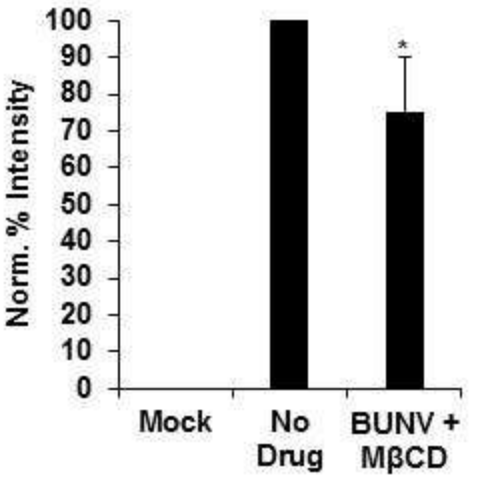
C
Norm. % Intensity
100
90
80
70
60
50
40
30
20
10
0
*
Mock
No Drug
BUNV + MßCD

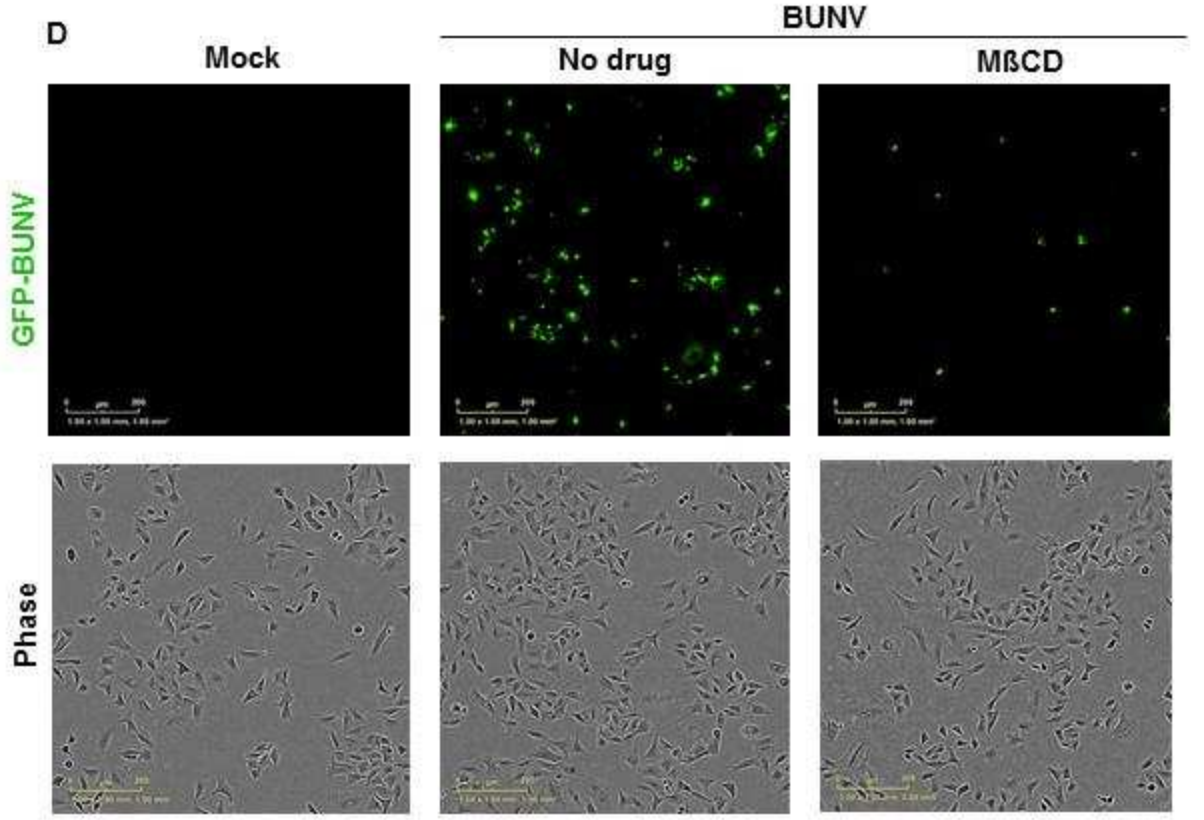
D
Mock
BUNV
No drug
MßCD
GFP-BUNV
Phase

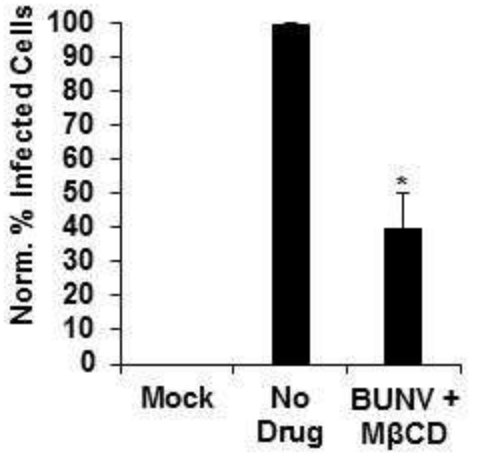
E
Norm. % Infected Cells
100
90
80
70
60
50
40
30
20
10
0
*
Mock
No Drug
BUNV + MßCD

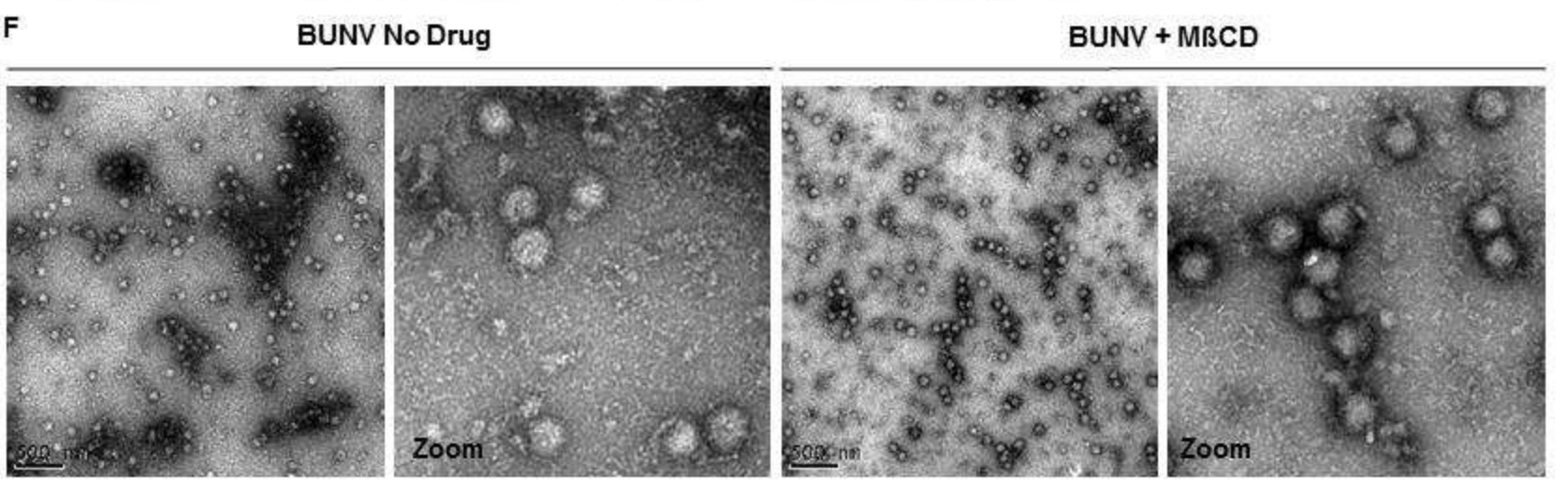
F
BUNV No Drug
BUNV + MßCD
Zoom
Zoom

A

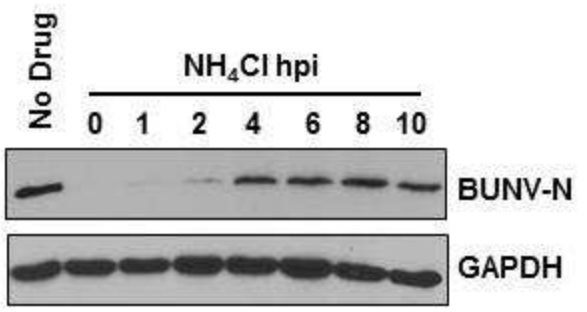
No Drug
NH4Cl hpi
0 1 2 4 6 8 10
BUNV-N
GAPDH

B

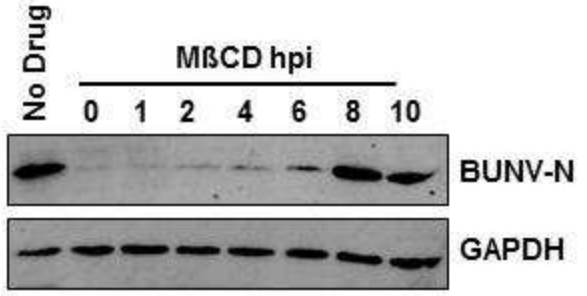
No Drug
MßCD hpi
0 1 2 4 6 8 10
BUNV-N
GAPDH

C

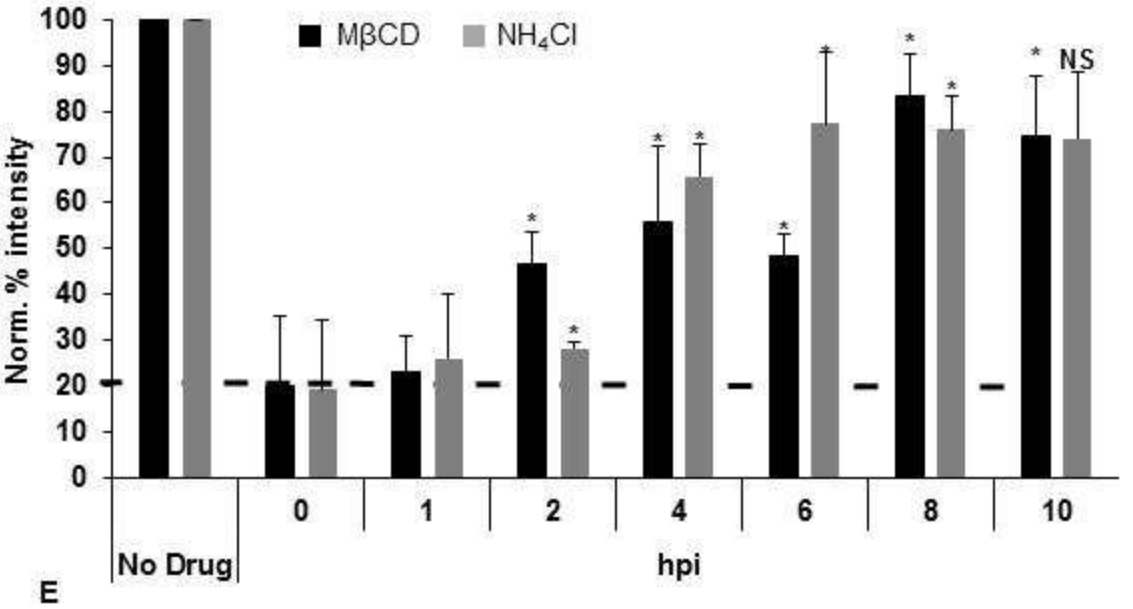
MβCD
NH4Cl
Norm. % intensity
100
90
80
70
60
50
40
30
20
10
0
NS
No Drug
0
1
2
4
6
8
10
hpi

D

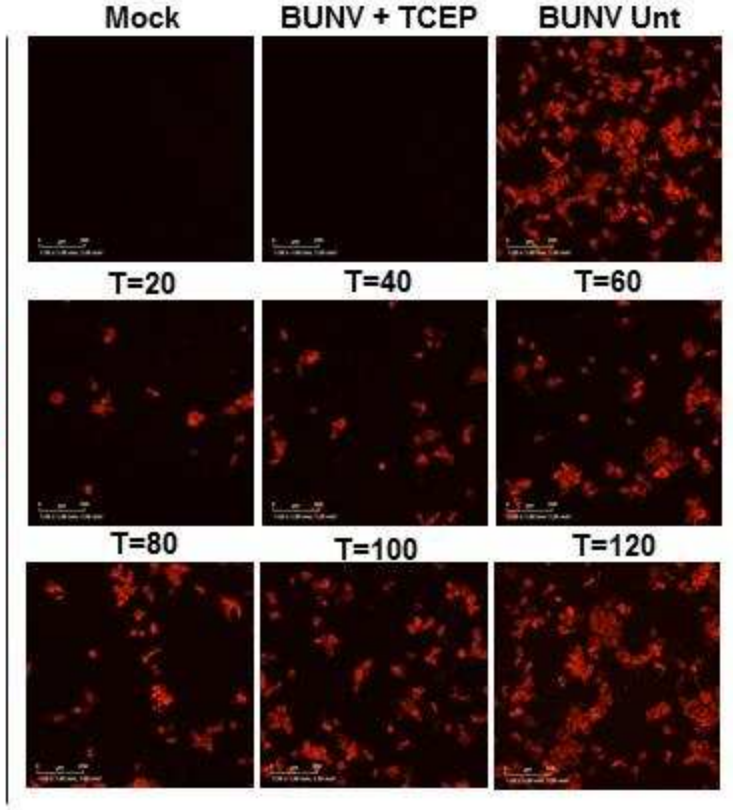
Mock
BUNV + TCEP
BUNV Unt
T=20
T=40
T=60
T=80
T=100
T=120
BUNV-N

E

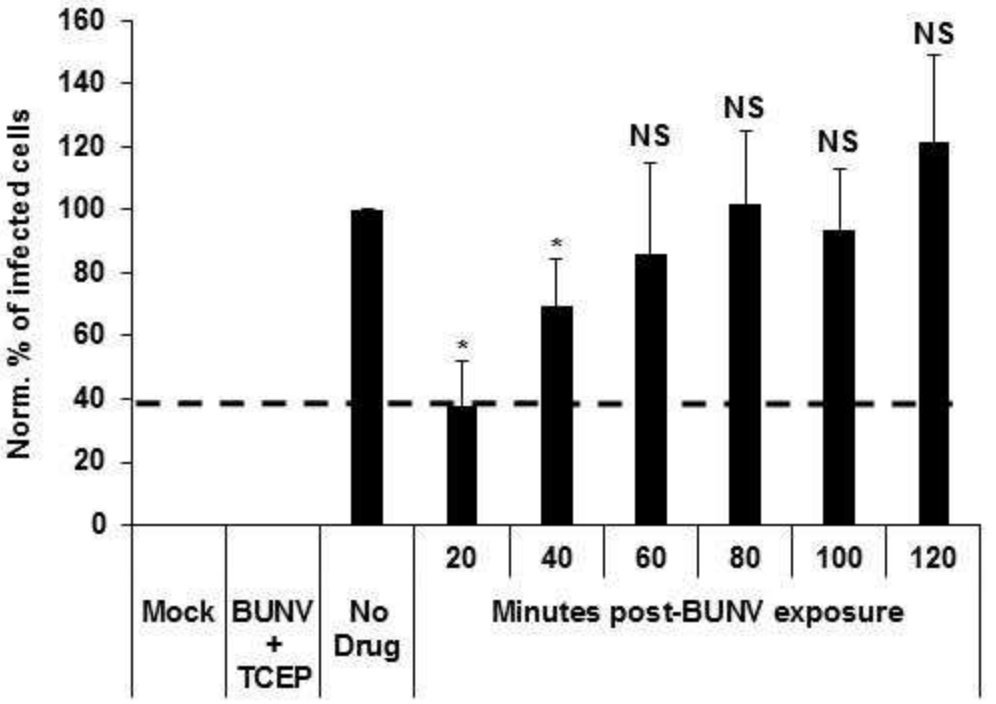
Norm. % of infected cells
160
140
120
100
80
60
40
20
0
NS
NS
NS
NS
Mock
BUNV + TCEP
No Drug
20
40
60
80
100
120
Minutes post-BUNV exposure

F

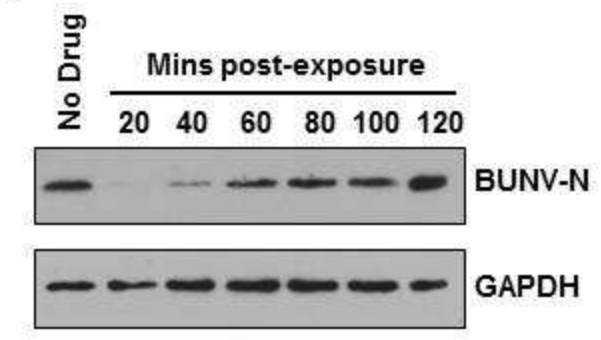
No Drug
Mins post-exposure
20 40 60 80 100 120
BUNV-N
GAPDH

G

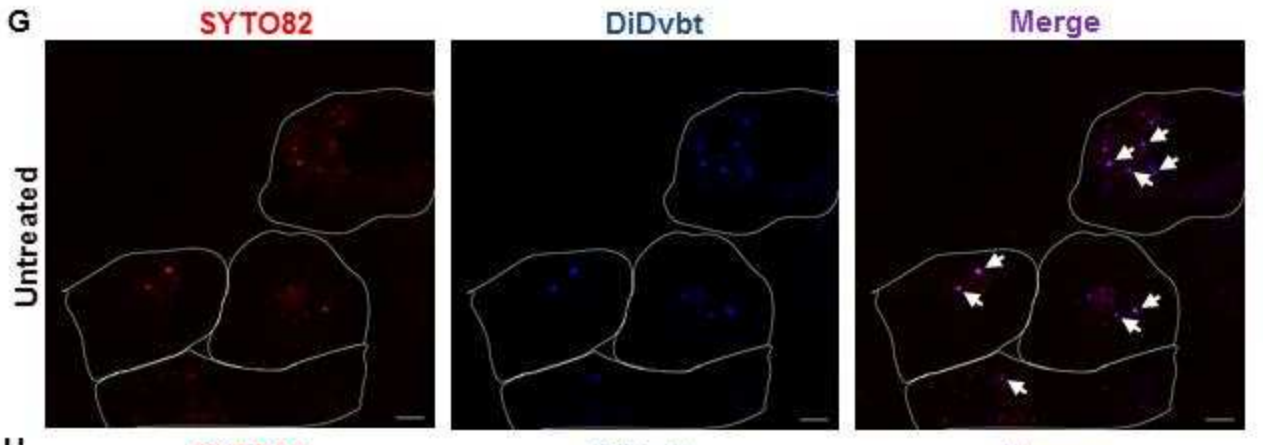
SYTO82
DiDvbt
Merge
Untreated

H

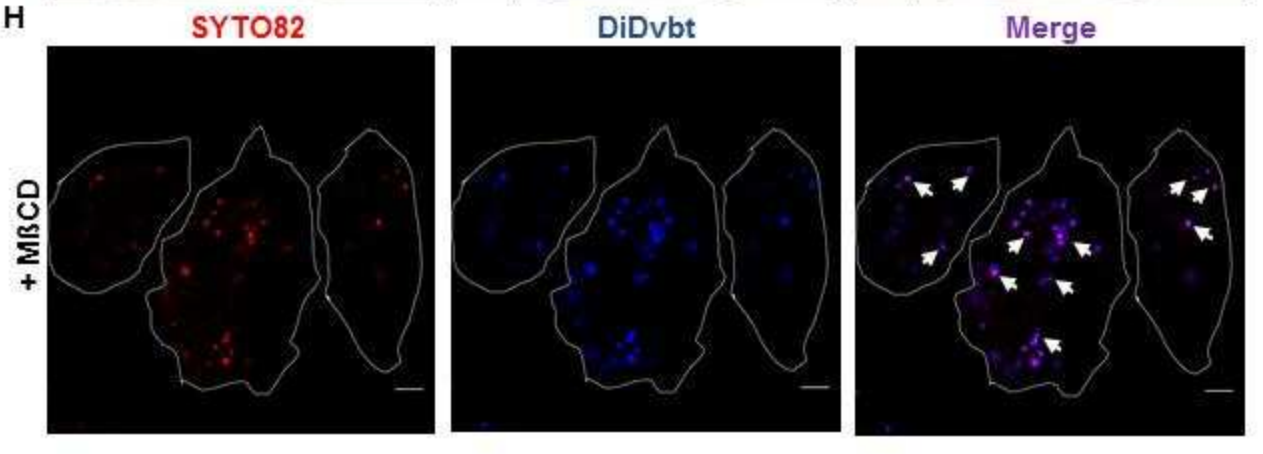
SYTO82
DiDvbt
Merge
+ MßCD

A

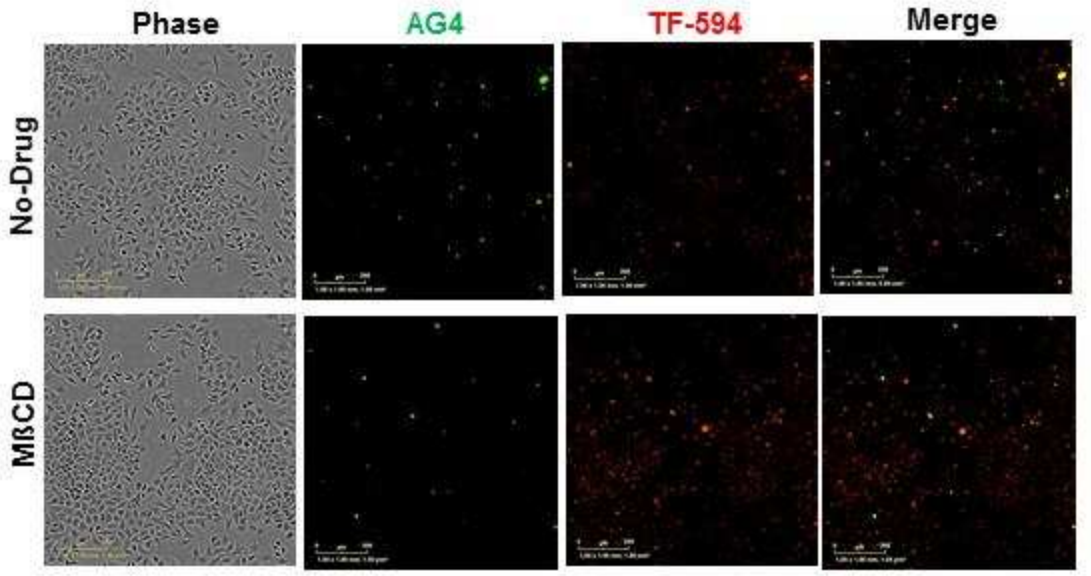
Phase
AG4
TF-594
Merge
No-Drug
MßCD

B

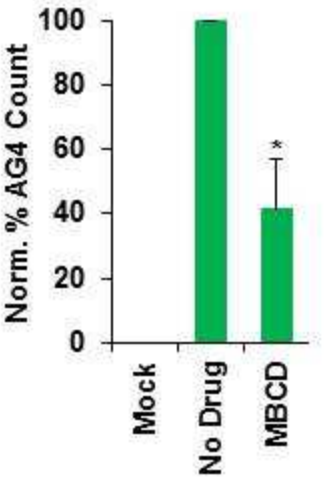
Norm. % AG4 Count
100
80
60
40
20
0
*
Mock
No Drug
MBCD

C

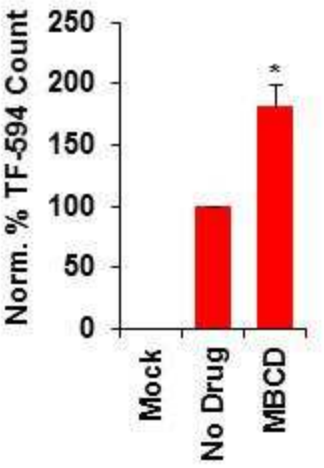
Norm. % TF-594 Count
250
200
150
100
50
0
*
Mock
No Drug
MBCD

D

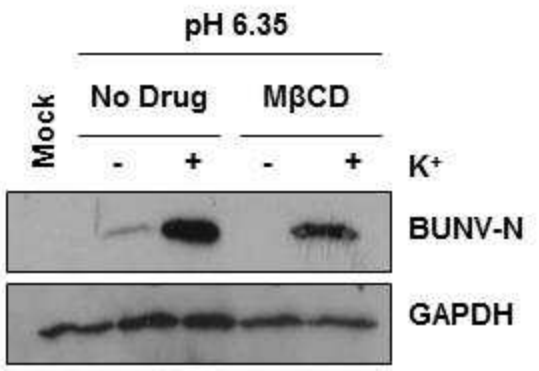
pH 6.35
Mock
No Drug
MβCD
-
+
-
+
K+
BUNV-N
GAPDH

E

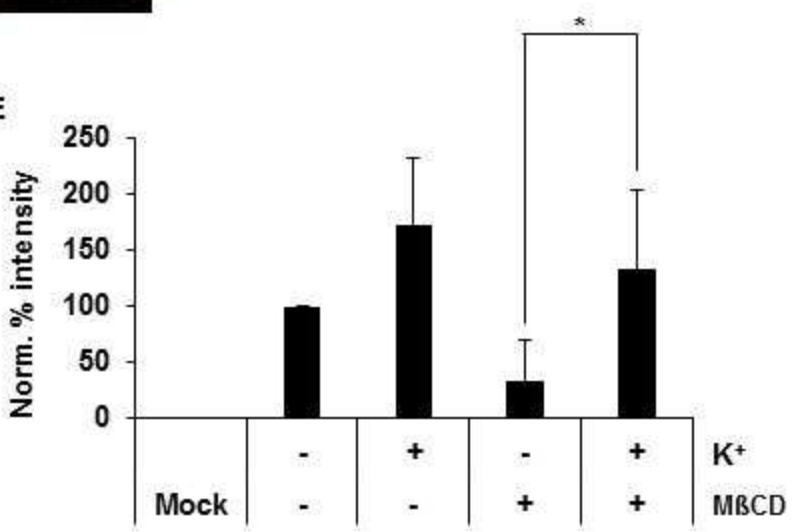
Norm. % intensity
250
200
150
100
50
0
*
-
+
-
+
K+
Mock
-
-
+
+
MßCD

F

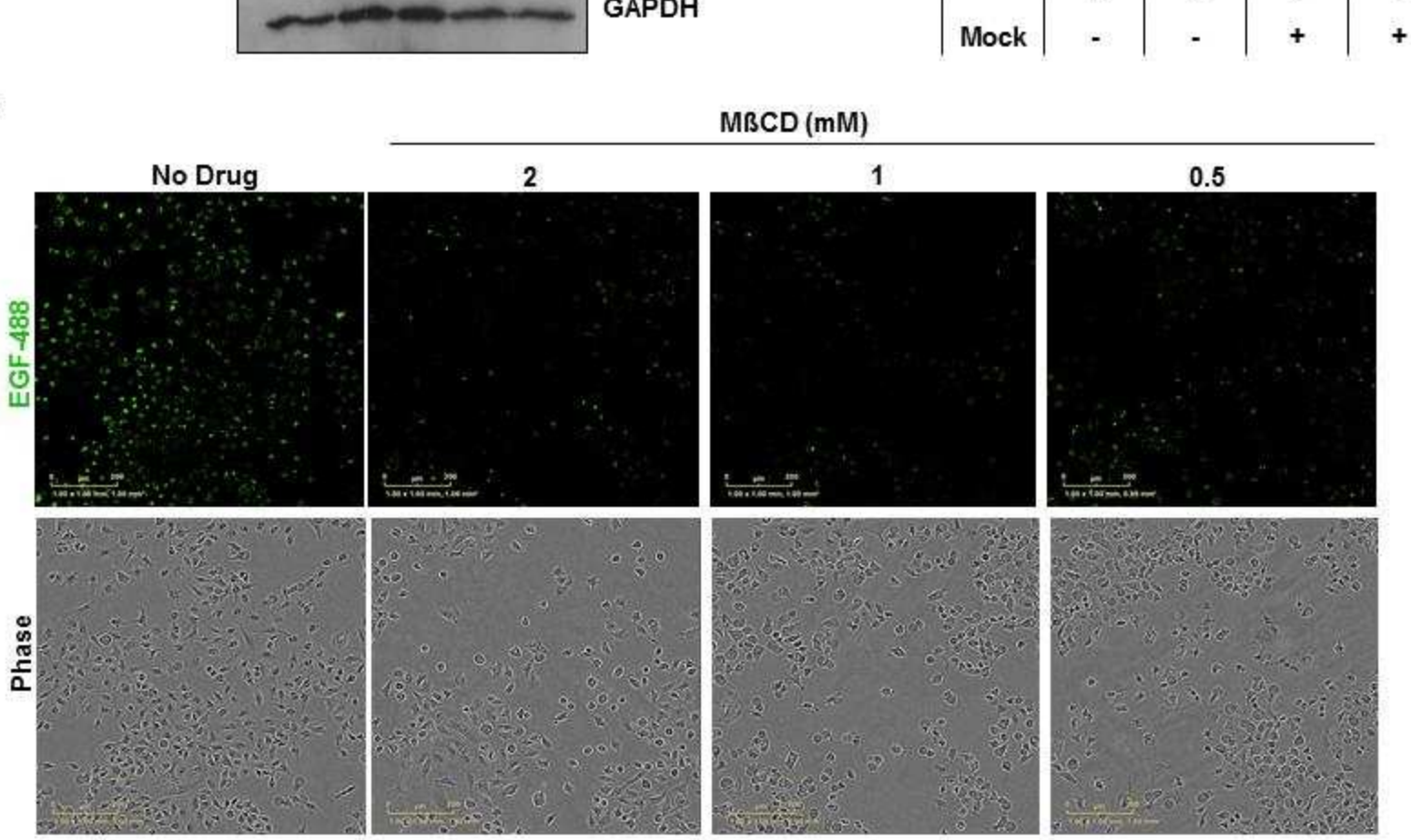
MßCD (mM)
No Drug
2
1
0.5
EGF-488
Phase

A

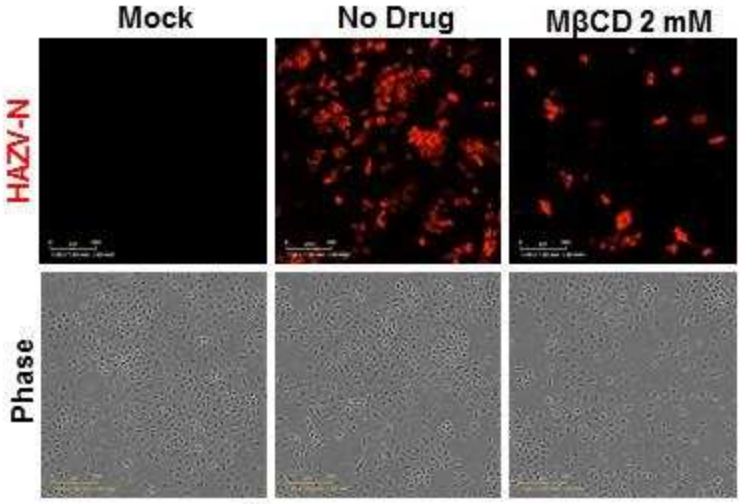

B

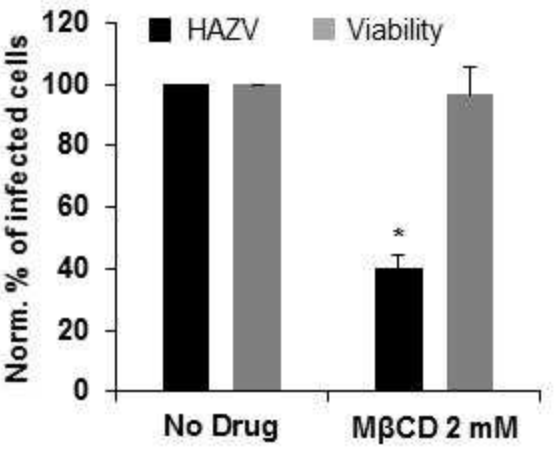

C

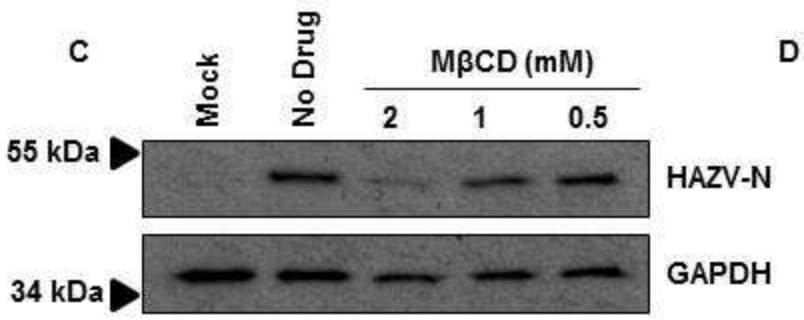

D

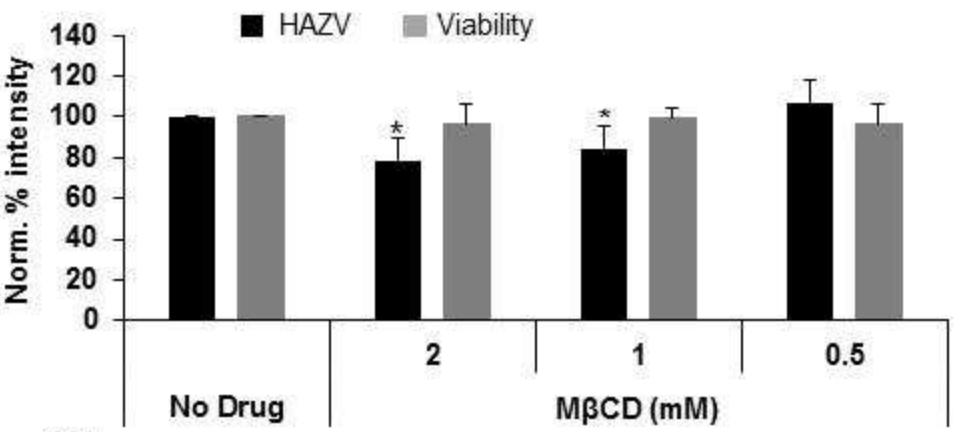

E

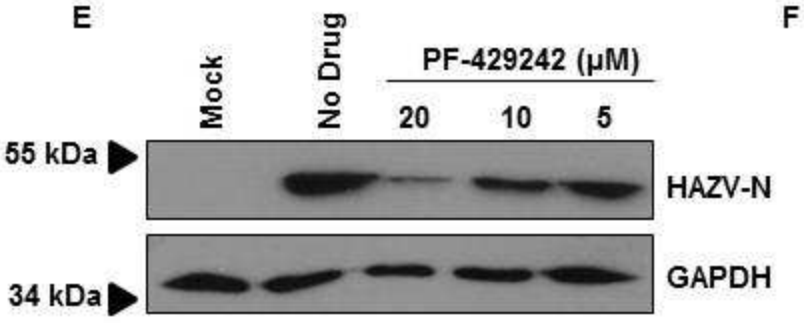

F

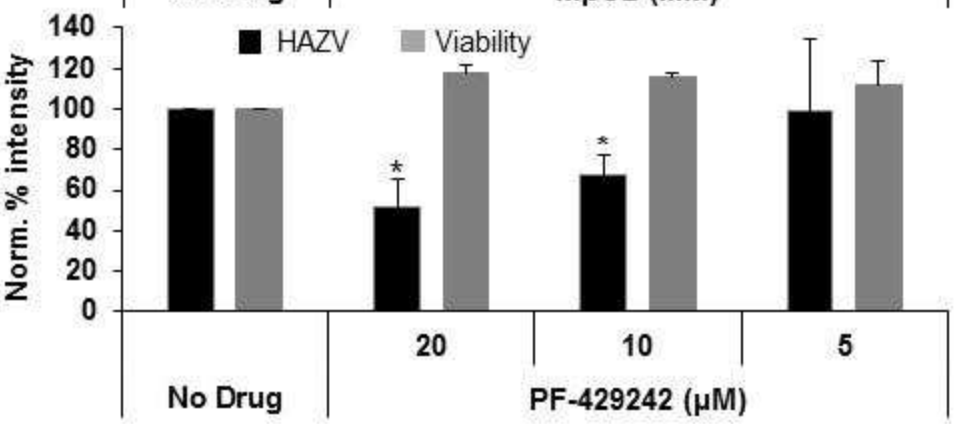

G

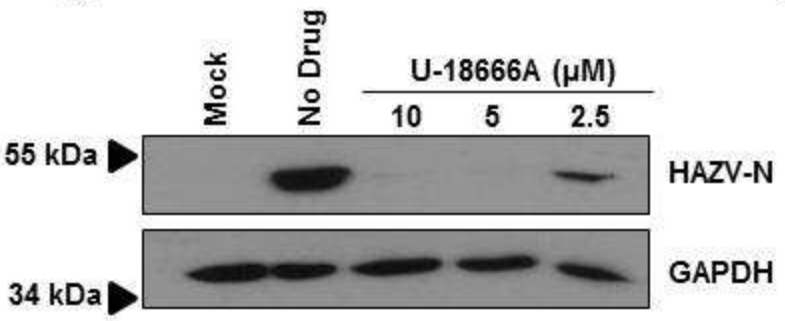

H

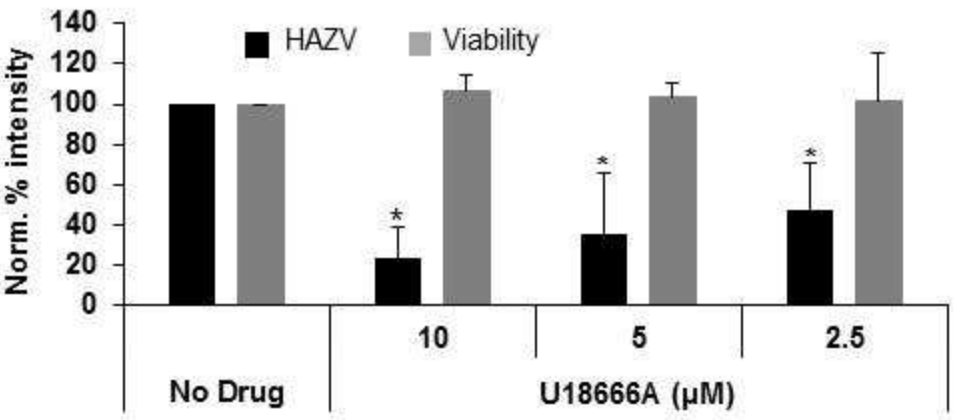

I

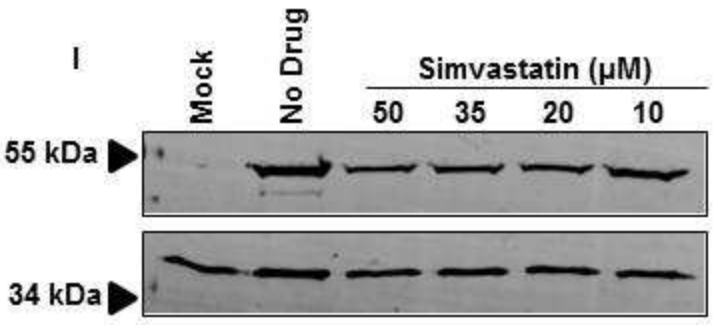

J

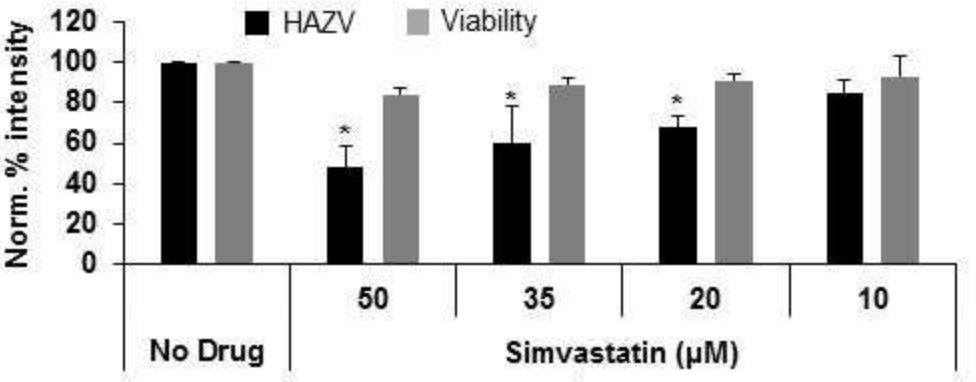

K

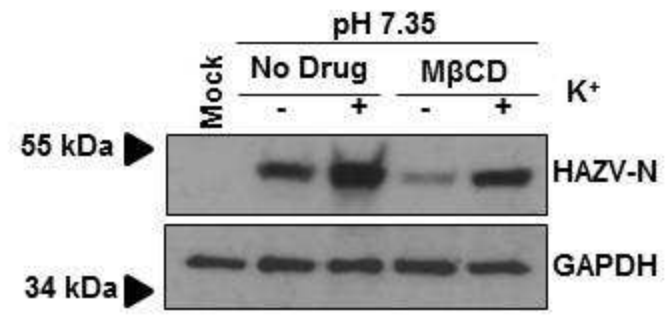

L

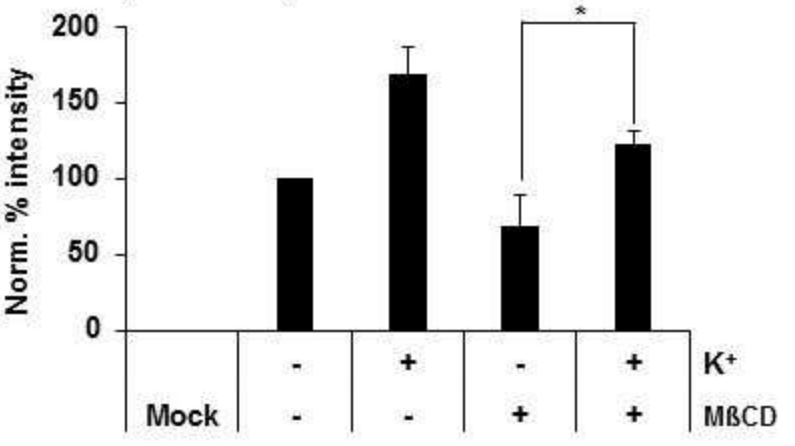

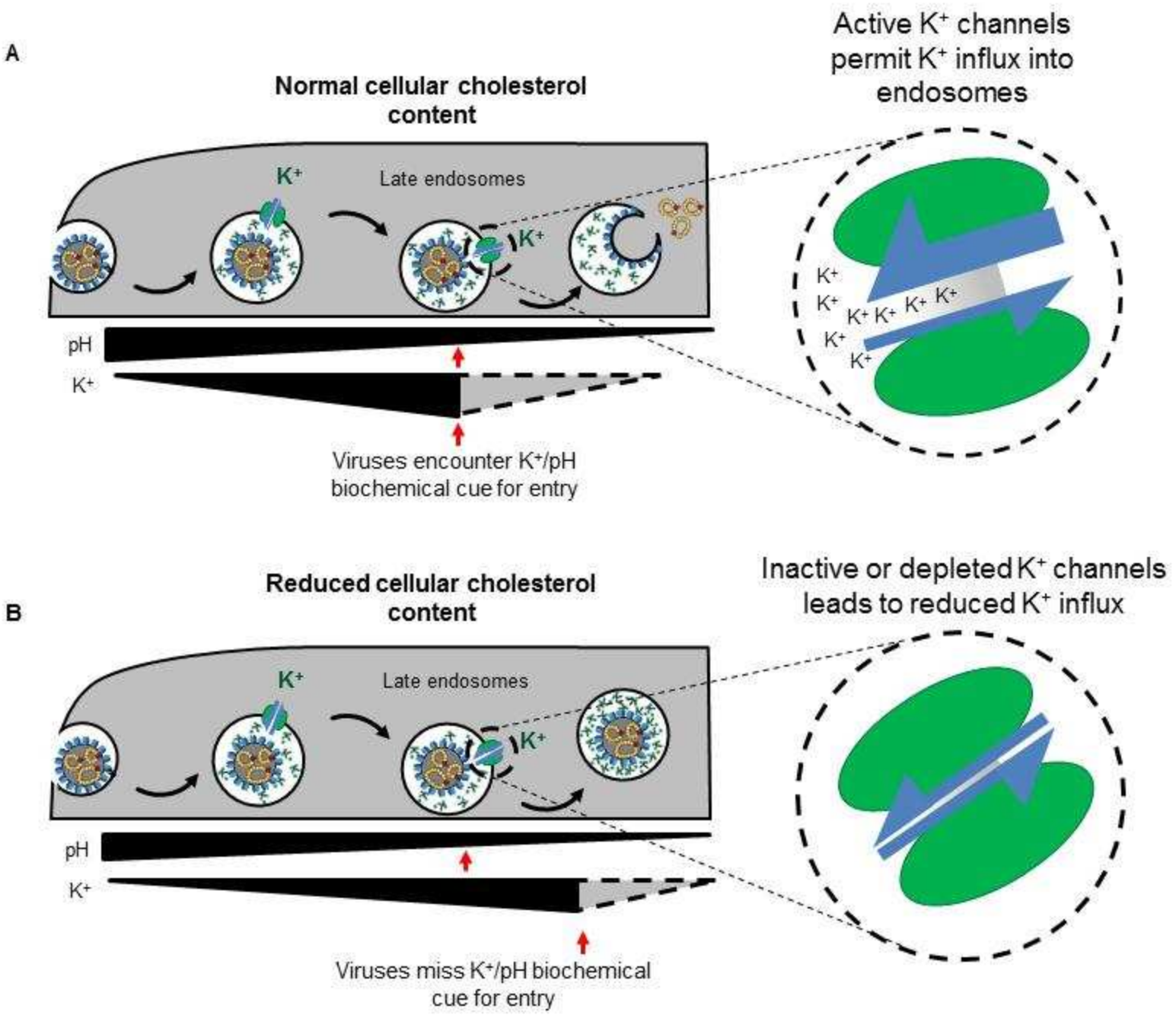
A
Normal cellular cholesterol content
Active K+ channels permit K+ influx into endosomes
K+
Late endosomes
K+
pH
K+
K+
K+
K+ K+ K+ K+
K+
K+
Viruses encounter K+/pH biochemical cue for entry
B
Reduced cellular cholesterol content
Inactive or depleted K+ channels leads to reduced K+ influx
K+
Late endosomes
K+
pH
K+
Viruses miss K+/pH biochemical cue for entry